Towards the Classification of Tachyon-Free Models From Tachyonic Ten-Dimensional Heterotic String Vacua

Alon E. Faraggi[*], Viktor G. Matyas[†] and Benjamin Percival[‡]

Dept. of Mathematical Sciences, University of Liverpool, Liverpool L69 7ZL, UK

Abstract

Recently it was proposed that ten-dimensional tachyonic string vacua may serve as starting points for the construction of viable four dimensional phenomenological string models which are tachyon free. This is achieved by projecting out the tachyons in the four-dimensional models using projectors other than the projector which is utilised in the supersymmetric models and those of the $SO(16) \times SO(16)$ heterotic string. We continue the exploration of this class of models by developing systematic computerised tools for their classification, the analysis of their tachyonic and massless spectra, as well as analysis of their partition functions and vacuum energy. We explore a randomly generated space of 2×10^9 string vacua in this class and find that tachyon–free models occur with $\sim 5 \times 10^{-3}$ probability, and of those, phenomenologically inclined $SO(10)$ vacua with $a_{00} = N_b^0 - N_f^0 = 0$, *i.e.* equal number of fermionic and bosonic massless states, occur with frequency $\sim 2 \times 10^{-6}$. Extracting larger numbers of phenomenological vacua therefore requires adaptation of fertility conditions that we discuss, and significantly increase the frequency of tachyon–free models. Our results suggest that spacetime supersymmetry may not be a necessary ingredient in phenomenological string models, even at the Planck scale.

[*]E-mail address: alon.faraggi@liv.ac.uk
[†]E-mail address: viktor.matyas@liv.ac.uk
[‡]E-mail address: benjamin.percival@liv.ac.uk

1　Introduction

String theory provides the tools to explore the connection of quantum gravity with cosmological and particle physics data. For that purpose we need to construct toy models that mimic the Standard Models of particle physics and cosmology. The heterotic string [1] is particularly appealing in this regard since it gives rise to $SO(10)$ Grand Unified Theory structures that are motivated by the Standard Model data. Since the mid–eighties the majority of string models studied possessed $N = 1$ spacetime supersymmetry. This is partly motivated by the attractiveness of supersymmetry as an extension of the Standard Model. It has a mathematically appealing symmetry structure that in its local form requires spin 2 constituents. It alleviates the tension between the electroweak and gravitational scales, and facilitates electroweak symmetry breaking by dimensional transmutation and this breaking is compatible with the observed data. Furthermore, the observed Higgs mass is compatible with low scale supersymmetry and indicates that the electroweak symmetry breaking mechanism is perturbative. From the point of view of string constructions, $N = 1$ supersymmetry guarantees that the vacuum is stable and simplifies the analysis of the spectra of string models. It is clear, however, that supersymmetry has to be broken at some scale, and despite its attractive features, its realisation at low scales is not mandatory.

Non–supersymmetric string models have also been of interest over the years. Those studies have mostly focused on analysing compactifications of the tachyon–free ten dimensional $SO(16) \times SO(16)$ heterotic string [2, 3, 4, 5, 6, 7]. In addition to the supersymmetric, and non–supersymmetric $SO(16) \times SO(16)$, models, heterotic string theory gives rise to models that are tachyonic in ten dimensions [2, 8, 9]. Recently, it was argued that these ten dimensional tachyonic vacua can also serve as good starting points for constructing tachyon free phenomenologically viable models [10, 11]. Whereas in the supersymmetric and non–supersymmetric $SO(16) \times SO(16)$ heterotic string the ten dimensional tachyons are projected out by the same projectors, they can be projected in the four dimensional models by using alternative projectors. Furthermore, a phenomenologically viable model was presented in ref. [11], and it was argued that in that specific example all the moduli, aside from the dilaton, are fixed perturbatively, and the dilaton may be fixed by the racetrack mechanism [12]. Hence, it was suggested that the model is stable, although it was acknowledged that discussions of stability in non–supersymmetric string vacua are at best speculative. Nevertheless, it illustrates the motivation to analyse the ten dimensional tachyonic vacua, on par with their supersymmetric and non–supersymmetric ten dimensional counterparts. Extending the construction of phenomenological models to this class of string compactifications may also shed light on some of the outstanding issues in string phenomenology.

Since the late eighties the heterotic string models in the free fermionic formulation [13] have provided a laboratory to study how the parameters of the Standard Model are determined in a theory of quantum gravity [14, 15, 16, 17, 18, 20, 21, 22, 23, 24, 25]. These models correspond to $Z_2 \times Z_2$ toroidal orbifold compactifications with discrete Wilson lines [26], and are related to compactifications on Z_2 orbifolds of $K_3 \times T_2$ manifolds. They give rise to a rich symmetry structure from a purely mathematical point of view [27]. Ultimately, this rich symmetry structure may be reflected in the physical properties of these string vacua, which is of future research interest. Three generation string models, with the $SO(10)$ GUT embedding of the Standard Model spectrum, were constructed

by following two routes. The first, the NAHE–based models, use a common subset of boundary condition basis vectors, the NAHE–set [28], which is extended by three or four additional basis vectors. Using this method, models with different unbroken $SO(10)$ subgroups were constructed [14, 15, 16, 17, 18]. The second route provides a powerful classification method of the $Z_2 \times Z_2$ toroidal orbifolds with different $SO(10)$ subgroups. The initial classification method was developed for vacua with unbroken $SO(10)$ subgroup [29, 30] and subsequently extended to models with Pati–Salam (PS) [20]; flipped $SU(5)$ (FSU5) [22]; Standard–like Model (SLM) [23]; and Left–Right Symmetric (LRS) [24, 25] $SO(10)$ subgroups. It led to the discovery of spinor–vector duality in the space of $(2, 0)$ string compactifications [30, 31, 32] and the existence of exophobic string vacua [20]. A NAHE–based tachyon–free three generation Standard–like Model that descends from a tachyonic ten-dimensional heterotic string vacuum was constructed in ref. [11]. The purpose of this paper is to initiate the systematic classification of tachyon–free models that descends from a particular class of tachyonic ten dimensional heterotic string vacuum. Toward this end, we limit the classification to models with unbroken $SO(10)$ subgroup, and extension to other subgroups is left for future work. We focus on the systematic analysis of the tachyonic and massless sectors in the models; and the systematic analysis of the partition function and the vacuum energy. We remark that in contrast to the supersymmetric models, systematic analysis of non–supersymmetric models requires separate analysis of the spacetime fermionic and bosonic sectors, as they are no longer related by the spacetime supersymmetric map. The computational time required is therefore doubled compared to supersymmetric models, which motivates the development of novel computational techniques [33]. In this regard, the direct analysis of the partition function provides a powerful complementary tool.

Our paper is organised as follows: in Section 2 we recap the main structure of the models that descend from the ten dimensional tachyonic vacua. The free fermionic classification method utilises a common set of boundary condition basis vectors, which is presented in Section 2, and the enumeration of the models is obtained by varying the one–loop Generalised GSO projection coefficients. We discuss in sections 2 and 5 two generic maps that play important roles in our analysis, the $\tilde{S}$–map (Section 2), and the $\tilde{x}$ map (Section 5). In Section 3 we discuss the gauge symmetry arising in our models and the sectors contributing to it. In sections 4 and 5 we set up the tools for the systematic analysis of the tachyonic and massless sectors of our models. In Section 6 discuss the systematic analysis of the partition function and the vacuum energy. In Section 7 we present the results of our classification. Section 8 concludes our paper with a discussion of the results and outlook for future research directions.

2   Ten Dimensional Vacua and the $\tilde{S}$-Map

In the free fermionic construction, models are specified in terms of boundary condition basis vectors and one–loop Generalised GSO (GGSO) phases [13]. The $E_8 \times E_8$ and $SO(16) \times SO(16)$ heterotic–models in ten dimensions are defined in terms of a common set of basis vectors

$$
\begin{aligned}
v_1 = \mathbb{1} &= \{\psi^\mu, \ \chi^{1,\dots,6} \mid \overline{\eta}^{1,2,3}, \overline{\psi}^{1,\dots,5}, \overline{\phi}^{1,\dots,8}\}, \\
v_2 = z_1 &= \{\overline{\psi}^{1,\dots,5}, \overline{\eta}^{1,2,3}\}, \\
v_3 = z_2 &= \{\overline{\phi}^{1,\dots,8}\},
\end{aligned}
\tag{2.1}
$$

where we adopted the common notation used in the free fermionic models [14, 17, 16, 18, 19, 20, 21, 22, 23, 24, 29, 30, 31]. The basis vector $\mathbb{1}$ is mandated by the modular invariance consistency rules [13], and produces a model with $SO(32)$ gauge symmetry from the Neveu-Schwarz (NS) sector. The spacetime supersymmetry generator arises from the combination

$$S = \mathbb{1} + z_1 + z_2 = \{\psi^\mu, \chi^{1,\dots,6}\}. \tag{2.2}$$

The choice of GGSO phase $C\begin{bmatrix} z_1 \\ z_2 \end{bmatrix} = \pm 1$ differentiates between the $SO(16) \times SO(16)$ or $E_8 \times E_8$ heterotic strings in ten dimensions. Eq. (2.2) dictates that in ten dimensions the breaking of spacetime supersymmetry is correlated with the breaking pattern $E_8 \times E_8 \to SO(16) \times SO(16)$. Equation (2.2) does not hold in lower dimensions, and the two breakings are not correlated. On the other hand, these vacua with broken and unbroken supersymmetry can be interpolated [34].

The tachyonic states in the $E_8 \times E_8$ and $SO(16) \times SO(16)$ heterotic strings in ten dimensions are projected out. The would–be tachyons in these models are obtained from the Neveu-Schwarz (NS) sector, by acting on the right–moving vacuum with a single fermionic oscillator

$$|0\rangle_L \otimes \bar{\phi}^a |0\rangle_R, \tag{2.3}$$

where in ten dimensions $a = 1, \cdots, 16$. The GSO projection induced by the S–vector projects out the untwisted tachyons, producing tachyon free models in both cases. As discussed in refs. [10, 11], obtaining the ten dimensional tachyonic vacua in the free fermionic formulation amounts to the removal of the S–vector from the construction. The ten dimensional configurations are obtained by substituting the z_1 basis vector with $z_1 = \{\bar{\phi}^{1,\cdots,4}\}$ and adding similar z_i basis vectors, with four periodic fermions, and at most two overlapping. These vacua are connected by interpolations or orbifolds along the lines of ref. [9], and, in general, contain tachyons in their spectrum.

In the free fermionic formulation, the four dimensional models that descend from the ten dimensional tachyonic vacua amount to removing the vector S from the set of basis vectors that are used to generate the models. In four spacetime dimensions the set $\{\mathbb{1}, z_1, z_2\}$ produces a non–supersymmetric model with $SU(2)^6 \times SO(12) \times E_8 \times E_8$ or $SU(2)^6 \times SO(12) \times SO(16) \times SO(16)$. An alternative to removing the S–vector from the construction is to augment it with periodic right–moving fermions. A convenient choice is given by

$$\tilde{S} = \{\psi^{1,2}, \chi^{1,2}, \chi^{3,4}, \chi^{5,6} \mid \bar{\phi}^{3,\cdots,6}\} \equiv 1 . \tag{2.4}$$

In this case there are no massless gravitinos, and the untwisted tachyonic states

$$|0\rangle_L \otimes \bar{\phi}^{3,\cdots,6} |0\rangle_R \tag{2.5}$$

are invariant under the $\tilde{S}$–vector projection. These untwisted tachyons are those that descend from the ten dimensional vacuum, hence confirming that the model can be regarded as a compactification of a ten dimensional tachyonic vacuum.

We therefore observe a general map, which is induced by the exchange

$$S \longleftrightarrow \tilde{S}, \tag{2.6}$$

in the construction of the heterotic string models that descend from the ten dimensional tachyonic vacua. We refer to this map as the $\tilde{S}$–map. It was discussed and used in the construction of the $\overline{\text{NAHE}}$–based model in ref. [11]. We remark that the $\tilde{S}$–map is

3

reminiscent of the map used to induce the spinor–vector duality in ref. [30, 32], in the sense that both utilise a block of four periodic right–moving worldsheet fermions. We may term these sorts of maps as modular maps, in the sense that they involve a block of four periodic complex worldsheet fermions. We therefore have another instance where such a modular map is reflected in the symmetry structure of the string vacua. Be it the spacetime supersymmetry in the models in which the S–basis vector is the supersymmetry spectral flow operator, or in the spinor–vector dual models in which a similar spectral flow operator operates in the observable E_8 sector and induces the spinor–vector duality map [30, 32]. Here, a similar operation is at play in the four dimensional models inducing the transformation from the supersymmetric (and non–supersymmetric) models that contain the S–basis vector, to the non–supersymmetric models that contain the $\tilde{S}$–basis vector. As discussed in ref. [35], this may be a reflection of a larger symmetry structure that underlies these models and string compactifications in general.

3 Non–Supersymmetric $SO(10)$ Models in 4D

Let us now define the classification structure for the $SO(10)$ models we consider, which employ the $\tilde{S}$–map. The first ingredient we need is a set of basis vectors that generate the space of $SO(10)$ $\tilde{S}$-models. We can choose the set

$$
\begin{aligned}
\mathbb{1} &= \{\psi^\mu,\ \chi^{1,\dots,6}, y^{1,\dots,6}, w^{1,\dots,6} \mid \overline{y}^{1,\dots,6}, \overline{w}^{1,\dots,6}, \overline{\psi}^{1,\dots,5}, \overline{\eta}^{1,2,3}, \overline{\phi}^{1,\dots,8}\}, \\
\tilde{S} &= \{\psi^\mu, \chi^{1,\dots,6} \mid \overline{\phi}^{3,4,5,6}\}, \\
e_i &= \{y^i, w^i \mid \overline{y}^i, \overline{w}^i\}, \quad i = 1, \dots, 6 \\
b_1 &= \{\psi^\mu, \chi^{12}, y^{34}, y^{56} \mid \overline{y}^{34}, \overline{y}^{56}, \overline{\eta}^1, \overline{\psi}^{1,\dots,5}\}, \\
b_2 &= \{\psi^\mu, \chi^{34}, y^{12}, y^{56} \mid \overline{y}^{12}, \overline{y}^{56}, \overline{\eta}^2, \overline{\psi}^{1,\dots,5}\}, \\
b_3 &= \{\psi^\mu, \chi^{56}, y^{12}, y^{34} \mid \overline{y}^{12}, \overline{y}^{34}, \overline{\eta}^3, \overline{\psi}^{1,\dots,5}\}, \\
z_1 &= \{\overline{\phi}^{1,\dots,4}\},
\end{aligned}
\tag{3.1}
$$

which is a similar basis set to $\overline{\text{NAHE}}=\{\mathbb{1}, \tilde{S}, b_1, b_2, b_3\}$ employed in [11], except with the inclusion of z_1 to break the hidden gauge group and of e_i to obtain all symmetric shifts of the internal $\Gamma_{6,6}$ lattice. We note that the vector b_3 which spans the third twisted plane and facilitates the analysis of the obervable spinorial representations is typically formed as a linear combination in previous supersymmetric classifications [29, 30, 20, 22, 23, 24, 25]. Furthermore we note the existence of a vector combination z_2

$$
z_2 = \mathbb{1} + \sum_{i=1}^{6} e_i + \sum_{k=1}^{3} b_k + z_1 = \{\overline{\phi}^{5,6,7,8}\}
\tag{3.2}
$$

in our models, which is typically its own basis vector in previous classifications.

Models may then be defined through the specification of GGSO phases $C\begin{bmatrix} v_i \\ v_j \end{bmatrix}$, which for our $SO(10)$ models are 66 free phases with all others specified by modular invariance. Hence, the full space of models is of size $2^{66} \sim 10^{19.9}$ models. This is a notably enlarged space compared with the supersymmetric $SO(10)$ case where the requirement that the spectrum is supersymmetric fixes some GGSO phases.

4

With a basis and a set of GGSO phases, we can construct the modular invariant Hilbert space $\mathcal{H}$ of states $|S_\alpha\rangle$ of the model through the one-loop GGSO projection such that

$$\mathcal{H} = \bigoplus_{\alpha \in \Xi} \prod_{i=1}^{k} \left\{ e^{i\pi v_i \cdot F_\alpha} |S_\alpha\rangle = \delta_\alpha C \begin{bmatrix} \alpha \\ v_i \end{bmatrix}^* |S_\alpha\rangle \right\} \tag{3.3}$$

where α is a sector formed as a linear combination of the basis vectors, F_α is the fermion number operator and $\delta_\alpha = 1, -1$ is the spin-statistics index.

The sectors in the model can be characterised according to the left and right moving vacuum separately

$$M_L^2 = -\frac{1}{2} + \frac{\alpha_L \cdot \alpha_L}{8} + N_L \tag{3.4}$$

$$M_R^2 = -1 + \frac{\alpha_R \cdot \alpha_R}{8} + N_R$$

where N_L and N_R are sums over left and right moving oscillators, respectively. Physical states must then additionally satisfy the Virasoro matching condition: $M_L^2 = M_R^2$, states not satisfying this correspond to off-shell states.

The untwisted sector gauge vector bosons for this choice of basis vectors give rise to a gauge group

$$SO(10) \times U(1)_1 \times U(1)_2 \times U(1)_3 \times SO(4)^4 \tag{3.5}$$

where our desired GUT $SO(10)$ is generated by the spacetime vector bosons $\psi^\mu \bar{\psi}^a \bar{\psi}^b |0\rangle$, the $U(1)_{i=1,2,3}$ are those generated by the worldsheet currents $: \bar{\eta}^i \bar{\eta}^{i*} :$ and the $SO(4)^4$ is the hidden sector generated by spacetime vector bosons from the pairs of $\bar{\phi}^a$ with common boundary conditions for each basis vector: $\{\bar{\phi}^{1,2}, \bar{\phi}^{3,4}, \bar{\phi}^{5,6}, \bar{\phi}^{7,8}\}$.

The gauge group of a model may be enhanced by additional gauge bosons which may arise from the z_1, z_2 and $z_1 + z_2$ sectors with appropriate oscillators, i.e.

$$\left\{ \begin{array}{c} \psi^\mu |z_1\rangle_L \otimes \{\bar{\lambda}^i\} |z_1\rangle_R \\ \psi^\mu |z_2\rangle_L \otimes \{\bar{\lambda}^i\} |z_2\rangle_R \\ \psi^\mu |z_1 + z_2\rangle_L \otimes |z_1 + z_2\rangle_R \end{array} \right\} \tag{3.6}$$

where $\bar{\lambda}^i$ are all possible right moving Neveu-Schwarz oscillators

Whether these gauge bosons appear is model-dependent since it depends on their survival under the GGSO projections. These enhancement sectors are also present in the familiar supersymmetric classification set-ups used in [29, 20, 22, 23, 24, 25]. However in those cases there is also an observable enhancement from the vector $x = \{\bar{\psi}^{1,...,5}, \bar{\eta}^{1,2,3}\}$, which arises as a linear combination in these models. If present, this vector induces the enhancement $SO(10) \times U(1) \rightarrow E_6$, where the $U(1) = U(1)_1 + U(1)_2 + U(1)_3$ combination is typically anomalous [37], unless such an enhancement is present. This result was first discussed in the context of the NAHE models, where including x in the basis was shown to similarly produce E_6 GUT models [38]. We therefore can see that one effect of our $\tilde{S}$ models with the basis (3.1) is to preclude the possibility of an E_6 enhancement in these models.

From (3.6) we can deduce that enhancements of the observable $SO(10)$ gauge group may arise from the sectors $\psi^\mu \{\bar{\psi}^a\} |z_1\rangle, \psi^\mu \{\bar{\psi}^a\} |z_2\rangle$, $a = 1, ..., 5$. Interestingly, the sectors: $|z_1\rangle, |z_2\rangle$ (with no oscillators) produce level-matched tachyons with conformal weight $(-1/2, -1/2)$ and so the appearance of these enhancements is correlated with the projection of level-matched tachyons. The full analysis of the level-matched tachyonic sectors is presented in the following section.

4 Tachyonic Sectors Analysis

Due to the absence of the supersymmetry generating vector S in our construction, analysing whether on-shell tachyons arise in the spectrum of our models becomes paramount. On-shell tachyons will arise when

$$M_L^2 = M_R^2 < 0, \qquad (4.1)$$

which corresponds to left and right products of $\alpha_L \cdot \alpha_L = 0, 1, 2, 3$ and $\alpha_R \cdot \alpha_R = 0, 1, 2, 3, 4, 5, 6, 7$. The presence of such tachyonic sectors in the physical spectrum indicates the instability of the string vacuum. There are 126 of these sectors in our models which are summarised compactly in Table 1. We will find that models in which all 126 on-

Mass Level	Vectorials	Spinorials
$(-1/2, -1/2)$	$\{\bar{\lambda}^m\}\,\|0\rangle$	$z_1,\; z_2$
$(-3/8, -3/8)$	$\{\bar{\lambda}^m\}e_i$	$e_i + z_1,\; e_i + z_2$
$(-1/4, -1/4)$	$\{\bar{\lambda}^m\}e_i + e_j$	$e_i + e_j + z_1,\; e_i + e_j + z_2$
$(-1/8, -1/8)$	$\{\bar{\lambda}^m\}e_i + e_j + e_k$	$e_i + e_j + e_k + z_1,\; e_i + e_j + e_k + z_2$

Table 1: *Level-matched tachyonic sectors and their mass level, where $i \neq j \neq k = 1, ..., 6$ and $\bar{\lambda}^m$ is any right-moving complex fermion with NS boundary condition for the relevant tachyonic sector.*

shell tachyons are projected by the GGSO projections appear with probability ~ 0.0054 and so in our classification we will throw away all but around 1 in 185 models.

In [7] a basis was chosen such that, rather than having the six internal shift vectors e_i, the combinations $T_1 = e_1 + e_2$, $T_2 = e_3 + e_4$ and $T_3 = e_5 + e_6$ were employed. Such a grouping does not allow for sectors to arise for all shifts in the internal space and, for example, means that spinorial $\mathbf{16}/\overline{\mathbf{16}}$ sectors have a degeneracy of 4 making 3 particle generations impossible once the $SO(10)$ group is broken. However, choosing $T_{i=1,2,3}$ did have the advantage of restricting the number of tachyonic sectors and allowing for a more simplified set-up to perform an analysis of the structure of the 1-loop potential in these models.

Since finding models in which all on-shell tachyons are projected is of utmost importance for all questions of stability of our string vacua we will delineate the methodology used in our analysis. In order to perform this analysis an efficient computer algorithm had to be developed which could scan samples of $\mathcal{O}(10^9)$ or more for on-shell tachyons within a reasonable computing time. The code we developed in python when running in parallel across 64 cores could check a sample of 10^9 models for tachyons in approximately 12 hours. A more detailed analysis of how to check whether our on-shell tachyons are projected is presented in the next section.

4.1 Note on the proto-graviton

Before we turn to the on-shell tachyon analysis we recall a general result first discussed in [36], which states that every non-supersymmetric string model necessarily contains off-shell tachyonic states with conformal weight $(0, -1)$. In our models these are

$$\psi^\mu \,|0\rangle_L \otimes |0\rangle_R\,, \qquad (4.2)$$

which will appear in the spectrum independent of the GGSO coefficients. We call such a state a "proto-graviton" and its guaranteed presence in the string spectrum can be understood at the CFT level by noting that it appears in the same Verma module as the graviton state which is always present in the massless NS sector.

4.2 Tachyons of conformal weight $(-\frac{1}{2}, -\frac{1}{2})$

The first on-shell tachyons we will inspect are those with conformal weight $(-\frac{1}{2}, -\frac{1}{2})$. Firstly we have the aforementioned untwisted tachyons (2.5) which are always projected since $\binom{z_1}{NS} = \binom{z_2}{NS} = -\binom{b_i}{NS} = 1$. Then there are then two spinorial tachyonic sectors at this mass level: z_1 and z_2. The conditions for their survival can be displayed as Tables 2 and 3.

Sector	$C\begin{bmatrix} z_1 \\ e_1 \end{bmatrix}$	$C\begin{bmatrix} z_1 \\ e_2 \end{bmatrix}$	$C\begin{bmatrix} z_1 \\ e_3 \end{bmatrix}$	$C\begin{bmatrix} z_1 \\ e_4 \end{bmatrix}$	$C\begin{bmatrix} z_1 \\ e_5 \end{bmatrix}$	$C\begin{bmatrix} z_1 \\ e_6 \end{bmatrix}$	$C\begin{bmatrix} z_1 \\ b_1 \end{bmatrix}$	$C\begin{bmatrix} z_1 \\ b_2 \end{bmatrix}$	$C\begin{bmatrix} z_1 \\ b_3 \end{bmatrix}$	$C\begin{bmatrix} z_1 \\ z_2 \end{bmatrix}$
z_1	+	+	+	+	+	+	+	+	+	+

Table 2: *Conditions on GGSO coefficients for survival of the on-shell tachyons $|z_1\rangle$*

Sector	$C\begin{bmatrix} z_2 \\ e_1 \end{bmatrix}$	$C\begin{bmatrix} z_2 \\ e_2 \end{bmatrix}$	$C\begin{bmatrix} z_2 \\ e_3 \end{bmatrix}$	$C\begin{bmatrix} z_2 \\ e_4 \end{bmatrix}$	$C\begin{bmatrix} z_2 \\ e_5 \end{bmatrix}$	$C\begin{bmatrix} z_2 \\ e_6 \end{bmatrix}$	$C\begin{bmatrix} z_2 \\ b_1 \end{bmatrix}$	$C\begin{bmatrix} z_2 \\ b_2 \end{bmatrix}$	$C\begin{bmatrix} z_2 \\ b_3 \end{bmatrix}$	$C\begin{bmatrix} z_2 \\ z_1 \end{bmatrix}$
z_2	+	+	+	+	+	+	+	+	+	+

Table 3: *Conditions on GGSO coefficients for survival of the on-shell tachyons $|z_2\rangle$*

Which tells us that only when all 10 of the column phases are +1 do the sectors remain in the spectrum. Interestingly, this has a bearing on the existence of the gauge group enhancements mentioned in the previous section. In particular, the only observable enhancements: $\psi^\mu |z_1\rangle_L \otimes \bar{\psi}^a |z_1\rangle$ and $\psi^\mu |z_2\rangle_L \otimes \bar{\psi}^a |z_2\rangle$ have the same survival conditions as the z_1, z_2 tachyonic sectors. Therefore we find that for our construction, there are no tachyon-free models in which the $SO(10)$ is enhanced. This is evident in the classification results shown in Table 14 of Section 7.

4.3 Tachyons of conformal weight $(-\frac{3}{8}, -\frac{3}{8})$

Now moving up the mass levels to $(-\frac{3}{8}, -\frac{3}{8})$, we have vectorial tachyons from the 6 sectors: $\{\bar{\lambda}^i\} |e_i\rangle$, $i = 1, ..., 6$ and spinorial tachyons from 12 sectors: $|e_i + z_1\rangle$ and $|e_i + z_2\rangle$. To demonstrate how to check the survival of these sectors we take the case of $\{\bar{\lambda}^i\} |e_1\rangle$, $|e_1 + z_1\rangle$ and $|e_1 + z_2\rangle$, which we show in the Tables 4, 5 and 6. The other cases with $e_{2,...,6}$ are much the same except for a simple permutation of the projection phases.

$\|e_1\rangle$ **Oscillator**	$C\begin{bmatrix}e_1\\\tilde{S}\end{bmatrix}$	$C\begin{bmatrix}e_1\\e_2\end{bmatrix}$	$C\begin{bmatrix}e_1\\e_3\end{bmatrix}$	$C\begin{bmatrix}e_1\\e_4\end{bmatrix}$	$C\begin{bmatrix}e_1\\e_5\end{bmatrix}$	$C\begin{bmatrix}e_1\\e_6\end{bmatrix}$	$C\begin{bmatrix}e_1\\b_1\end{bmatrix}$	$C\begin{bmatrix}e_1\\\tilde{x}\end{bmatrix}$	$C\begin{bmatrix}e_1\\z_1\end{bmatrix}$	$C\begin{bmatrix}e_1\\z_2\end{bmatrix}$
$\{\bar{y}^2\}$	+	-	+	+	+	+	-	+	+	+
$\{\bar{w}^2\}$	+	-	+	+	+	+	+	+	+	+
$\{\bar{y}^3\}$	+	+	-	+	+	+	-	+	+	+
$\{\bar{w}^3\}$	+	+	-	+	+	+	+	+	+	+
$\{\bar{y}^4\}$	+	+	+	-	+	+	-	+	+	+
$\{\bar{w}^4\}$	+	+	+	-	+	+	+	+	+	+
$\{\bar{y}^5\}$	+	+	+	+	-	+	-	+	+	+
$\{\bar{w}^5\}$	+	+	+	+	-	+	+	+	+	+
$\{\bar{y}^6\}$	+	+	+	+	+	-	-	+	+	+
$\{\bar{w}^6\}$	+	+	+	+	+	-	+	+	+	+
$\{\bar{\psi}^{1/2/3/4/5(*)}\}$ $/\{\bar{\eta}^{1(*)}\}$	+	+	+	+	+	+	-	-	+	+
$\{\bar{\eta}^{2,3(*)}\}$	+	+	+	+	+	+	+	-	+	+
$\{\bar{\phi}^{1,2(*)}\}$	+	+	+	+	+	+	+	+	-	+
$\{\bar{\phi}^{3,4(*)}\}$	-	+	+	+	+	+	+	+	-	+
$\{\bar{\phi}^{5,6(*)}\}$	-	+	+	+	+	+	+	+	+	-
$\{\bar{\phi}^{7,8(*)}\}$	+	+	+	+	+	+	+	+	+	-

Table 4: *Conditions on GGSO coefficients for survival of the on-shell vectorial tachyons $\{\bar{\lambda}^i\}\,|e_1\rangle$. We have made use of the combination $\tilde{x} = b_1 + b_2 + b_3 = \{\psi^\mu, \chi^{1,\dots,6} \mid \bar{\psi}^{1,2,3,4,5}, \bar{\eta}^{1,2,3}\}$, which will be discussed more in the next section.*

Sector	$C\begin{bmatrix}e_1+z_1\\e_2\end{bmatrix}$	$C\begin{bmatrix}e_1+z_1\\e_3\end{bmatrix}$	$C\begin{bmatrix}e_1+z_1\\e_4\end{bmatrix}$	$C\begin{bmatrix}e_1+z_1\\e_5\end{bmatrix}$	$C\begin{bmatrix}e_1+z_1\\e_6\end{bmatrix}$	$C\begin{bmatrix}e_1+z_1\\b_1\end{bmatrix}$	$C\begin{bmatrix}e_1+z_1\\\tilde{x}\end{bmatrix}$	$C\begin{bmatrix}e_1+z_1\\z_2\end{bmatrix}$
$\|e_1 + z_1\rangle$	+	+	+	+	+	+	+	+

Table 5: *Conditions on GGSO coefficients for survival of the on-shell tachyons $|e_1 + z_1\rangle$*

Sector	$C\begin{bmatrix}e_1+z_2\\e_2\end{bmatrix}$	$C\begin{bmatrix}e_1+z_2\\e_3\end{bmatrix}$	$C\begin{bmatrix}e_1+z_2\\e_4\end{bmatrix}$	$C\begin{bmatrix}e_1+z_2\\e_5\end{bmatrix}$	$C\begin{bmatrix}e_1+z_2\\e_6\end{bmatrix}$	$C\begin{bmatrix}e_1+z_2\\b_1\end{bmatrix}$	$C\begin{bmatrix}e_1+z_2\\\tilde{x}\end{bmatrix}$	$C\begin{bmatrix}e_1+z_2\\z_1\end{bmatrix}$
$\|e_1 + z_2\rangle$	+	+	+	+	+	+	+	+

Table 6: *Conditions on GGSO coefficients for survival of the on-shell tachyons $|e_1 + z_2\rangle$*

4.4 Tachyons of conformal weight $(-\frac{1}{4}, -\frac{1}{4})$

Carrying on up the mass levels we have $(-\frac{1}{4}, -\frac{1}{4})$ in which vectorial tachyons arise from 15 sectors: $\{\bar{\lambda}^i\}\,|e_i + e_j\rangle$, $i \neq j = 1, \dots, 6$ and spinorial tachyons arise from 30 sectors: $|e_i + e_j + z_1\rangle$ and $|e_i + e_j + z_2\rangle$. Again, we will present the conditions on the survival of $\{\bar{\lambda}^i\}\,|e_1 + e_2\rangle$, $|e_1 + e_2 + z_1\rangle$ and $|e_1 + e_2 + z_2\rangle$ in Tables 7, 8 and 9 below and note that the other sectors with other e_i combinations are easily obtainable from these.

$\lvert e_1+e_2\rangle$ **Oscillators**	$C\begin{bmatrix}e_1+e_2\\\tilde{S}\end{bmatrix}$	$C\begin{bmatrix}e_1+e_2\\e_3\end{bmatrix}$	$C\begin{bmatrix}e_1+e_2\\e_4\end{bmatrix}$	$C\begin{bmatrix}e_1+e_2\\e_5\end{bmatrix}$	$C\begin{bmatrix}e_1+e_2\\e_6\end{bmatrix}$	$C\begin{bmatrix}e_1+e_2\\b_1\end{bmatrix}$	$C\begin{bmatrix}e_1+e_2\\\tilde{x}\end{bmatrix}$	$C\begin{bmatrix}e_1+e_2\\z_1\end{bmatrix}$	$C\begin{bmatrix}e_1+e_2\\z_2\end{bmatrix}$
$\{\bar{y}^3\}$	+	-	+	+	+	-	+	+	+
$\{\bar{w}^3\}$	+	-	+	+	+	+	+	+	+
$\{\bar{y}^4\}$	+	+	-	+	+	-	+	+	+
$\{\bar{w}^4\}$	+	+	-	+	+	+	+	+	+
$\{\bar{y}^5\}$	+	+	+	-	+	-	+	+	+
$\{\bar{w}^5\}$	+	+	+	-	+	+	+	+	+
$\{\bar{y}^6\}$	+	+	+	+	-	-	+	+	+
$\{\bar{w}^6\}$	+	+	+	+	-	+	+	+	+
$\{\bar{\psi}^{1/.../5(*)}\}$ $/\{\bar{\eta}^{1(*)}\}$	+	+	+	+	+	-	-	+	+
$\{\bar{\eta}^{2,3(*)}\}$	+	+	+	+	+	+	-	+	+
$\{\bar{\phi}^{1,2(*)}\}$	+	+	+	+	+	+	+	-	+
$\{\bar{\phi}^{3,4(*)}\}$	-	+	+	+	+	+	+	-	+
$\{\bar{\phi}^{5,6(*)}\}$	-	+	+	+	+	+	+	+	-
$\{\bar{\phi}^{7,8(*)}\}$	+	+	+	+	+	+	+	+	-

Table 7: *Conditions on GGSO coefficients for survival of the on-shell vectorial tachyons* $\{\bar{\lambda}^i\}\lvert e_1+e_2\rangle$. *We have made use of the combination* $\tilde{x}=b_1+b_2+b_3=\{\psi^\mu,\chi^{1,...,6}\mid\bar{\psi}^{1,2,3,4,5},\bar{\eta}^{1,2,3}\}$, *which will be discussed more in the next section.*

Sector	$C\begin{bmatrix}e_1+e_2+z_1\\e_3\end{bmatrix}$	$C\begin{bmatrix}e_1+e_2+z_1\\e_4\end{bmatrix}$	$C\begin{bmatrix}e_1+e_2+z_1\\e_5\end{bmatrix}$	$C\begin{bmatrix}e_1+e_2+z_1\\e_6\end{bmatrix}$	$C\begin{bmatrix}e_1+e_2+z_1\\b_1\end{bmatrix}$	$C\begin{bmatrix}e_1+e_2+z_1\\\tilde{x}\end{bmatrix}$	$C\begin{bmatrix}e_1+e_2+z_1\\z_2\end{bmatrix}$
$\lvert e_1+e_2+z_1\rangle$	+	+	+	+	+	+	+

Table 8: *Conditions on GGSO coefficients for survival of the on-shell tachyons* $\lvert e_1+e_2+z_1\rangle$.

Sector	$C\begin{bmatrix}e_1+e_2+z_2\\e_3\end{bmatrix}$	$C\begin{bmatrix}e_1+e_2+z_2\\e_4\end{bmatrix}$	$C\begin{bmatrix}e_1+e_2+z_2\\e_5\end{bmatrix}$	$C\begin{bmatrix}e_1+e_2+z_2\\e_6\end{bmatrix}$	$C\begin{bmatrix}e_1+e_2+z_2\\b_1\end{bmatrix}$	$C\begin{bmatrix}e_1+e_2+z_2\\\tilde{x}\end{bmatrix}$	$C\begin{bmatrix}e_1+e_2+z_2\\z_1\end{bmatrix}$
$\lvert e_1+e_2+z_2\rangle$	+	+	+	+	+	+	+

Table 9: *Conditions on GGSO coefficients for survival of the on-shell tachyons* $\lvert e_1+e_2+z_2\rangle$.

4.5 Tachyons of conformal weight $\left(-\frac{1}{8},-\frac{1}{8}\right)$

The final mass level we obtain on-shell tachyons from is $\left(-\frac{1}{8},-\frac{1}{8}\right)$, where vectorial tachyons arise from 20 sectors: $\{\bar{\lambda}^i\}\lvert e_i+e_j+e_k\rangle$, $i\neq j\neq k=1,...,6$ and spinorial tachyons arise from 40 sectors: $\lvert e_i+e_j+e_k+z_1\rangle$ and $\lvert e_i+e_j+e_k+z_2\rangle$. We present the conditions on the survival of $\{\bar{\lambda}^i\}\lvert e_1+e_2+e_3\rangle$, $\lvert e_1+e_2+e_3+z_1\rangle$ and $\lvert e_1+e_2+e_3+z_2\rangle$ in the Tables 10, 11 and 12 below and note again that the conditions for other sectors with other e_i combinations are easily obtainable from these.

$\lvert e_1+e_2+e_3\rangle$ Oscillator	$C\begin{bmatrix}e_1+e_2+e_3\\ \tilde{S}\end{bmatrix}$	$C\begin{bmatrix}e_1+e_2+e_3\\ e_4\end{bmatrix}$	$C\begin{bmatrix}e_1+e_2+e_3\\ e_5\end{bmatrix}$	$C\begin{bmatrix}e_1+e_2+e_3\\ e_6\end{bmatrix}$	$C\begin{bmatrix}e_1+e_2+e_3\\ \tilde{x}\end{bmatrix}$	$C\begin{bmatrix}e_1+e_2+e_3\\ z_1\end{bmatrix}$	$C\begin{bmatrix}e_1+e_2+e_3\\ z_2\end{bmatrix}$
$\{\bar{y}^4/\bar{w}^4\}$	+	-	+	+	+	+	+
$\{\bar{y}^5/\bar{w}^5\}$	+	+	-	+	+	+	+
$\{\bar{y}^6/\bar{w}^6\}$	+	+	+	-	+	+	+
$\{\psi^{1/\ldots/5}\}$ $/\{\bar{\eta}^{1/2/3(*)}\}$	+	+	+	+	-	+	+
$\{\bar{\phi}^{1,2(*)}\}$	+	+	+	+	+	-	+
$\{\bar{\phi}^{3,4(*)}\}$	-	+	+	+	+	-	+
$\{\bar{\phi}^{5,6(*)}\}$	-	+	+	+	+	+	-
$\{\bar{\phi}^{7,8(*)}\}$	+	+	+	+	+	+	-

Table 10: *Conditions on GGSO coefficients for survival of the on-shell vectorial tachyons* $\{\bar{\lambda}^i\}\lvert e_1+e_2+e_3\rangle$.

Sector	$C\begin{bmatrix}e_1+e_2+e_3+z_1\\ e_4\end{bmatrix}$	$C\begin{bmatrix}e_1+e_2+e_3+z_1\\ e_5\end{bmatrix}$	$C\begin{bmatrix}e_1+e_2+e_3+z_1\\ e_6\end{bmatrix}$	$C\begin{bmatrix}e_1+e_2+e_3+z_1\\ \tilde{x}\end{bmatrix}$	$C\begin{bmatrix}e_1+e_2+e_3+z_1\\ z_2\end{bmatrix}$
$\lvert e_1+e_2+e_3+z_1\rangle$	+	+	+	+	+

Table 11: *Conditions on GGSO coefficients for survival of the on-shell tachyons* $\lvert e_1+e_2+e_3+z_1\rangle$.

Sector	$C\begin{bmatrix}e_1+e_2+e_3+z_2\\ e_4\end{bmatrix}$	$C\begin{bmatrix}e_1+e_2+e_3+z_2\\ e_5\end{bmatrix}$	$C\begin{bmatrix}e_1+e_2+e_3+z_2\\ e_6\end{bmatrix}$	$C\begin{bmatrix}e_1+e_2+e_3+z_2\\ \tilde{x}\end{bmatrix}$	$C\begin{bmatrix}e_1+e_2+e_3+z_2\\ z_1\end{bmatrix}$
$\lvert e_1+e_2+e_3+z_2\rangle$	+	+	+	+	+

Table 12: *Conditions on GGSO coefficients for survival of the on-shell tachyons* $\lvert e_1+e_2+e_3+z_2\rangle$.

Using this structure of the conditions on the GGSO phases for the survival of tachyonic sectors at each mass level our computer algorithm runs through and checks whether any configuration of the phases that leaves the tachyon in the spectrum is satisfied. If none are satisfied then all 126 are projected and the model is retained for further analysis.

Having dealt now with the $M_L^2 = M_R^2 < 0$ level-matched sectors we turn our attention to the more familiar discussion of the structure of the massless sectors $M_L^2 = M_R^2 = 0$ in the following section where we can discern the phenomenological features of our models.

5 Massless Sectors

Now that we have a way to generate models free of on-shell tachyons, we can turn our attention to the massless sectors and their representations. Although some aspects of the massless spectrum look similar to the supersymmetric case, the structure of our $\tilde{S}$-models are very different. In particular, we can contrast our models with those in which supersymmetry is spontaneously broken (by a GGSO phase) where in general some parts of the spectrum remain supersymmetric. This was, for example, demonstrated in [39] in terms of invariant orbits of the partition function for orbifold models with spontaneously broken supersymmetry. Similarly, our models are very different than those of the broken supersymmertry models discussed in [5] where observable spinorial sectors of the models still exhibit a supersymmetric–like structure, *i.e.* in these sectors the bosonic and fermionic

states only differ by their charges under some $U(1)$ symmetries that are broken at a high scale.

As we explore this new structure in the massless spectrum we will see that the role of the $\tilde{S}$-map is of central importance. Further to this, we will also uncover the importance of a vector combination $\tilde{x}$ which induces another interesting map. Without the presence of the supersymmetry generator S we must also handle a number of extra massless sectors which would not arise in supersymmetric setups due to the GGSO projections induced by S.

5.1 The Observable Sectors and the $\tilde{S}$ and $\tilde{x}$-maps

The chiral spinorial $\mathbf{16}/\overline{\mathbf{16}}$ representations arise from the 48 sectors (16 from each orbifold plane)

$$
\begin{aligned}
B^{(1)}_{pqrs} &= b_1 + pe_3 + qe_4 + re_5 + se_6 \\
&= \{\psi^\mu, \chi^{1,2}, (1-p)y^3\bar{y}^3, pw^3\bar{w}^3, (1-q)y^4\bar{y}^4, qw^4\bar{w}^4, \\
&\qquad (1-r)y^5\bar{y}^5, rw^5\bar{w}^5, (1-s)y^6\bar{y}^6, sw^6\bar{w}^6, \bar{\eta}^1, \bar{\psi}^{1,\dots,5}\} \\
B^{(2)}_{pqrs} &= b_2 + pe_1 + qe_2 + re_5 + se_6 \\
B^{(3)}_{pqrs} &= b_3 + pe_1 + qe_2 + re_3 + se_4
\end{aligned}
\tag{5.1}
$$

where $p, q, r, s = 0, 1$ account for all combinations of shift vectors of the internal fermions $\{y^i, w^i \mid \bar{y}^i, \bar{w}^i\}$. As in previous classifications, we can now write down generic algebraic equations to determine the number $\mathbf{16}$ and $\overline{\mathbf{16}}$, $N_{\mathbf{16}}$ and $N_{\overline{\mathbf{16}}}$, as a function of the GGSO coefficients. To do this we first utilize the following projectors to determine which of the 48 spinorial sectors survive

$$
\begin{aligned}
P^1_{pqrs} &= \frac{1}{2^4} \prod_{i=1,2}\left(1 - C\begin{bmatrix} B^1_{pqrs} \\ e_i \end{bmatrix}^*\right) \prod_{a=1,2}\left(1 - C\begin{bmatrix} B^1_{pqrs} \\ z_a \end{bmatrix}^*\right) \\
P^2_{pqrs} &= \frac{1}{2^4} \prod_{i=3,4}\left(1 - C\begin{bmatrix} B^2_{pqrs} \\ e_i \end{bmatrix}^*\right) \prod_{a=1,2}\left(1 - C\begin{bmatrix} B^2_{pqrs} \\ z_a \end{bmatrix}^*\right) \\
P^3_{pqrs} &= \frac{1}{2^4} \prod_{i=5,6}\left(1 - C\begin{bmatrix} B^3_{pqrs} \\ e_i \end{bmatrix}^*\right) \prod_{a=1,2}\left(1 - C\begin{bmatrix} B^3_{pqrs} \\ z_a \end{bmatrix}^*\right)
\end{aligned}
\tag{5.2}
$$

where, we recall that the vector $z_2 = \{\bar{\phi}^{5,6,7,8}\}$ is the combination defined in eq. (3.2). Then we define the chirality phases

$$
\begin{aligned}
X^1_{pqrs} &= -C\begin{bmatrix} B^1_{pqrs} \\ b_2 + (1-r)e_5 + (1-s)e_6 \end{bmatrix}^* \\
X^2_{pqrs} &= -C\begin{bmatrix} B^2_{pqrs} \\ b_1 + (1-r)e_5 + (1-s)e_6 \end{bmatrix}^* \\
X^3_{pqrs} &= -C\begin{bmatrix} B^3_{pqrs} \\ b_1 + (1-r)e_3 + (1-s)e_4 \end{bmatrix}^*
\end{aligned}
\tag{5.3}
$$

11

to determine whether a sector will give rise to a **16** or a $\overline{\mathbf{16}}$. With these definitions we can write compact expressions for N_{16} and $N_{\overline{16}}$

$$N_{16} = \frac{1}{2} \sum_{\substack{A=1,2,3 \\ p,q,r,s=0,1}} P^A_{pqrs} \left(1 + X^A_{pqrs}\right)$$

$$N_{\overline{16}} = \frac{1}{2} \sum_{\substack{A=1,2,3 \\ p,q,r,s=0,1}} P^A_{pqrs} \left(1 - X^A_{pqrs}\right).$$

(5.4)

Up to here these equations are familiar from previous supersymmetric classifications. However there is a fundamental difference from the supersymmetric case where $B^{1,2,3}$, along with all model sectors, appear in supermultiplets with superpartners obtained through the addition of S, which exchanges spacetime bosons with spacetime fermions but leaves the gauge group representations unchanged. In our set-up, the fermionic $B^{1,2,3}$ sectors have no such bosonic sector counterparts. Indeed, the addition of our basis vector $\tilde{S}$ would give rise to massive states with non-trivial representations under the hidden sector gauge group. As mentioned above, we can also compare with the broken supersymmetry models of [5] where the bosonic counterparts of $B^{1,2,3}$ only differ from their fermionic superpartners by their charges under some $U(1)$ symmetries that are broken at a high scale.

A further new important feature of our construction is the inclusion of the vector

$$\tilde{x} = b_1 + b_2 + b_3$$

(5.5)

which we name in analogy to the x–vector from the supersymmetric classifications [30, 20, 22, 24, 25]. We note that $\tilde{x}$ is the same as the vector $S+x$ which arises in supersymmetric models. In these models the states from the x–sector enhances the observable gauge symmetry from $SO(10)$ to E_6, so $S + x$ arises when such an enhancement is present. The vector $\tilde{x}$ is important in our models since it plays the role of mapping between the observable spinorial and vectorial representations of $SO(10)$, as well as a map between bosonic and fermionic states. More specifically, the $\tilde{x}$–vector maps sectors that produce spacetime fermions in the spinorial representation of $SO(10)$, from which the Standard Model matter states are obtained, to sectors that produce spacetime bosons in its vectorial representation, from which the Standard Model Higgs state is obtained. Thus, the $\tilde{x}$–map induces simultaneously the fermion–boson map of the S–vector, as well as the spinor–vector map of the x–vector. Without S to provide the simple symmetry at each mass level between bosons and fermions the question of the relationship between bosons and fermions is unclear. It appears that the structure is controlled in some sense by the $\tilde{S}$-map and the $\tilde{x}$-map taking us between mass levels as both these maps often change the mass level of the sector they act on.

We also note that the $\tilde{x}$–sector also affects the observable spectrum since its presence in the Hilbert space results in an extra 4 **16**'s and $\overline{\mathbf{16}}$'s of $SO(10)$. The $\tilde{x}$–sector corresponds to the sector producing the fermionic superpartners of the states from the x–sector, *i.e.* $S + x$, which enhance the $SO(10)$ symmetry to E_6. The $\tilde{x}$–sector therefore gives rise to the fermionic superpartners of the spacetime vector bosons from the x–sector, which are in fact absent from the spectrum.

5.2 Vectorial Sectors

As mentioned above, the vector $\tilde{x}$ in (5.5) maps between the spinorial sectors $B_{pqrs}^{1,2,3}$ and vectorial sectors:

$$
\begin{aligned}
V_{pqrs}^{(1)} &= B_{pqrs}^{(1)} + \tilde{x} \\
&= b_2 + b_3 + pe_3 + qe_4 + re_5 + se_6 \\
&= \{\chi^{3,4,5,6}, (1-p)y^3\bar{y}^3, pw^3\bar{w}^3, (1-q)y^4\bar{y}^4, qw^4\bar{w}^4, \\
&\qquad (1-r)y^5\bar{y}^5, rw^5\bar{w}^5, (1-s)y^6\bar{y}^6, sw^6\bar{w}^6, \bar{\eta}^{2,3}\} \\
V_{pqrs}^{(2)} &= B_{pqrs}^{(2)} + \tilde{x} \\
V_{pqrs}^{(3)} &= B_{pqrs}^{(3)} + \tilde{x}
\end{aligned}
\tag{5.6}
$$

The observable vectorial **10** representations of $SO(10)$ arise when the right moving oscillator is a $\overline{\psi}^{a(*)}$, $a = 1, ..., 5$. To determine the number of such observable vectorial sectors we use the projectors

$$
\begin{aligned}
R_{pqrs}^{(1)} &= \frac{1}{2^4} \prod_{i=1,2}\left(1 + C\begin{bmatrix} e_i \\ V_{pqrs}^{(1)} \end{bmatrix}\right) \prod_{a=1,2}\left[1 + C\begin{bmatrix} z_a \\ V_{pqrs}^{(1)} \end{bmatrix}\right) \\
R_{pqrs}^{(2)} &= \frac{1}{2^4} \prod_{i=3,4}\left(1 + C\begin{bmatrix} e_i \\ V_{pqrs}^{(2)} \end{bmatrix}\right) \prod_{a=1,2}\left(1 + C\begin{bmatrix} z_a \\ V_{pqrs}^{(2)} \end{bmatrix}\right) \\
R_{pqrs}^{(3)} &= \frac{1}{2^4} \prod_{i=5,6}\left(1 + C\begin{bmatrix} e_i \\ V_{pqrs}^{(3)} \end{bmatrix}\right) \prod_{a=1,2}\left(1 + C\begin{bmatrix} z_a \\ V_{pqrs}^{(3)} \end{bmatrix}\right).
\end{aligned}
\tag{5.7}
$$

Using these we can write the number of vectorial **10**'s arising from these sectors as

$$
N_{10} = \sum_{\substack{A=1,2,3 \\ p,q,r,s=0,1}} R_{pqrs}^A.
\tag{5.8}
$$

Further to these observable vectorials arising from $V^{1,2,3}$ there are the additional states arising for the other choices of oscillator $\bar{y}_{NS}^i, \bar{w}_{NS}^i, \bar{\phi}^{1,2}, \bar{\phi}^{3,4}, \bar{\phi}^{5,6}, \bar{\phi}^{7,8}$, which only transform under the hidden group.

In contrast to the supersymmetric case, our models come with additional vectorial sectors, which can give rise to states transforming under the observable gauge group as well as the hidden.

Firstly we observe 4 additional sectors that can give rise to vectorial states transforming under both the observable and the hidden or solely the hidden. These sectors are

$$
\tilde{V} = \{\{\bar{\lambda}^i\}|\tilde{S}\rangle, \{\bar{\lambda}^i\}|\tilde{S}+z_1\rangle, \{\bar{\lambda}^i\}|\tilde{S}+z_2\rangle, \{\bar{\lambda}^i\}|\tilde{S}+z_1+z_2\rangle\}
\tag{5.9}
$$

which are spacetime fermions. There are two cases to distinguish when one of these sectors is present:

- $\{\bar{y}^i/\bar{w}^i\}|\tilde{V}\rangle$ which are charged under the hidden sector only.

- $\{\bar{\psi}^{1,...,5}, \bar{\eta}^{1,2,3}, \bar{\phi}_{NS}\}|\tilde{V}\rangle$ with $\bar{\phi}_{NS}$ being the four Neveu-Schwarz oscillators such that $\bar{\phi}_{NS} \cap \tilde{V} = \emptyset$. These transform in mixed representations of the observable and

hidden sectors which means we should analyse them further. We realise that the condition for one of these to remain in the spectrum is:

$$C\begin{bmatrix}\tilde{V}\\e_i\end{bmatrix} = -1, \quad \forall\, i \in \{1,2,3,4,5,6\} \tag{5.10}$$

for one of the $\tilde{V}$. In ref. [11] it was suggested that such states appearing in these models may be instrumental in implementing electroweak symmetry breaking by hidden sector condensates.

Similar to the $\tilde{x}$–sector, it is interesting to compare the $\tilde{S}$–sector with the S–sector in supersymmetric models. The S–sector in the supersymmetric models produces the spacetime fermionic superpartners of the states from the NS–sector, *i.e.* it gives rise to the gauginos. The $\tilde{S}$–sector gives rise to spacetime fermions that could transform as, *e.g.* electroweak doublets and triplets, but also transforms as doublets of the hidden gauge group, due to the $\tilde{S}$–map noted in Section 2. In this respect the $\tilde{S}$–models exhibit a sort of split supersymmetry, in the sense that the states from the sectors $B_{1,2,3}$ are massive, but the sector that produces the would–be gauginos, *i.e.* $\tilde{S}$, still produces massless states transforming under the observable gauge symmetry. It will be of interest to explore how this phenomenon affects the phenomenological characteristics of the models.

Finally, there are further vectorials that may be observable or hidden arising from the 15 sectors

$$\gamma^{k=1,\dots,15} = \{\bar{\lambda}^i\}\,|e_i + e_j + e_k + e_l\rangle \tag{5.11}$$

for $i \neq j \neq k \neq l = 1, \dots, 6$.

We note that these sectors can give rise to vectorial **10**'s when the oscillators $\bar{\psi}^a$, $a = 1, \dots, 5$, are present. In this case the projector is

$$P_{\gamma^k} = \frac{1}{2^5} \prod_{i=m,n}\left(1 + C\begin{bmatrix}\gamma^k\\e_i\end{bmatrix}\right) \prod_{a=1,2}\left(1 + C\begin{bmatrix}\gamma^k\\z_a\end{bmatrix}\right)\left(1 - C\begin{bmatrix}\gamma^k\\\tilde{x}\end{bmatrix}\right) \tag{5.12}$$

where $m \neq n \neq i \neq j \neq k \neq l$. We can count the number of such sectors through the expression

$$N_\gamma^{\{\bar{\psi},\bar{\eta}\}} = \sum_{k=1}^{15} P_{\gamma^k}. \tag{5.13}$$

These additional vectorials can evidently play a role in the phenomenology of our models, so their couplings and charge contributions must be considered carefully for specific models. We can note that γ^k will not couple at leading order to the observable spinorial representations due to their additional charges, and so at leading order the only vectorial 10 representations to generate realistic Standard Model fermion mass spectrum, remain those from $V^{1,2,3}$.

5.3 Hidden Sectors

We find that there are a relatively large number of hidden massless sectors in our model, which is another effect of the $\tilde{S}$-map we have chosen, since its right moving complex fermions generate representations of the hidden group.

Firstly, we can identify 96 spinorial sectors that give rise to spacetime bosons arising through the addition of z_1 or z_2 onto the vectorial sectors $V^{1,2,3}$

$$
\begin{aligned}
H^{(1)}_{pqrs} &= V^{(1)}_{pqrs} + z_1 \\
H^{(2)}_{pqrs} &= V^{(2)}_{pqrs} + z_1 \\
H^{(3)}_{pqrs} &= V^{(3)}_{pqrs} + z_1 \\
H^{(4)}_{pqrs} &= V^{(1)}_{pqrs} + z_2 \\
H^{(5)}_{pqrs} &= V^{(2)}_{pqrs} + z_2 \\
H^{(6)}_{pqrs} &= V^{(3)}_{pqrs} + z_2
\end{aligned}
\tag{5.14}
$$

which evidently transform under the hidden $SO(4)^4$ only.

A further four groups of 48 sectors are generated through the addition of the combinations $\{\tilde{S}, \tilde{S} + z_1, \tilde{S} + z_2, \tilde{S} + z_1 + z_2\}$ which give rise to spacetime fermionic hidden sectors:

$$
\begin{aligned}
H^{(7)}_{pqrs} &= \tilde{S} + V^{(1)}_{pqrs} \\
H^{(8)}_{pqrs} &= \tilde{S} + V^{(2)}_{pqrs} \\
H^{(9)}_{pqrs} &= \tilde{S} + V^{(3)}_{pqrs} \\
H^{(10)}_{pqrs} &= \tilde{S} + V^{(1)}_{pqrs} + z_1 \\
H^{(11)}_{pqrs} &= \tilde{S} + V^{(2)}_{pqrs} + z_1 \\
H^{(12)}_{pqrs} &= \tilde{S} + V^{(3)}_{pqrs} + z_1 \\
H^{(13)}_{pqrs} &= \tilde{S} + V^{(1)}_{pqrs} + z_2 \\
H^{(14)}_{pqrs} &= \tilde{S} + V^{(2)}_{pqrs} + z_2 \\
H^{(15)}_{pqrs} &= \tilde{S} + V^{(3)}_{pqrs} + z_2 \\
H^{(16)}_{pqrs} &= \tilde{S} + V^{(1)}_{pqrs} + z_1 + z_2 \\
H^{(17)}_{pqrs} &= \tilde{S} + V^{(2)}_{pqrs} + z_1 + z_2 \\
H^{(18)}_{pqrs} &= \tilde{S} + V^{(3)}_{pqrs} + z_1 + z_2
\end{aligned}
\tag{5.15}
$$

Essentially we see that by adding on the combinations: $\tilde{h}_n = \{z_1, z_2, \tilde{S}, \tilde{S} + z_1, \tilde{S} + z_2, \tilde{S} + z_1 + z_2\}$ we generate the 6 ways of having 2 doublet representations of the four hidden $SO(4)$ groups. Knowing the number of hidden sectors will mainly be useful when looking at the size of massless coefficient in the q-expansion of the partition function, which is equivalent to a counting of the number of massless states. We will return to this in Section 6.

There are additional hidden sectors, on top of those counted by N_H, that don't live on the orbifold planes. These 30 sectors are:

$$
\delta^{1,\ldots,30} = \begin{cases} e_i + e_j + e_k + e_l + z_1 \\ e_i + e_j + e_k + e_l + z_2 \end{cases}
\tag{5.16}
$$

for $i \neq j \neq k \neq l = 1, \ldots, 6$. Similar to (5.9), (5.11) these are examples of sectors which are not found in supersymmetric models since the S–vector would project them out. Again, in order to evaluate the massless contribution to the q-expansion we will need to count the states arising from these sectors.

6   Partition Function and Cosmological Constant

The partition function of string models encapsulates all the information one knows about its structure, symmetries and spectrum. Thus to fully understand our model it is essential to get a handle on the calculation and form of its partition function. The analysis of the partition function is particularly instrumental in non–supersymmetric constructions, since it gives a complementary tool to count the total number of massless states, and its integration over the fundamental domain correspond to the cosmological constant.

For free fermionic models, the partition function receives contributions from both the fermionic and bosonic coordinates. That is the partition function can be split into $Z = Z_B Z_F$. Since the fermions are free, their contribution to the partition function is purely determined in terms of their boundary conditions on the world-sheet torus, hence we can write

$$Z = Z_B \sum_{Sp.Str.} C\begin{bmatrix} \alpha \\ \beta \end{bmatrix} \prod_f Z\begin{bmatrix} \alpha(f) \\ \beta(f) \end{bmatrix}, \tag{6.1}$$

where α and β represent the boundary conditions, the sum is over all choices of spin structure and the product is over all fermions. The GGSO coefficients $C\begin{bmatrix} \alpha \\ \beta \end{bmatrix}$ are chosen so that Z_F is modular invariant. The $Z[\alpha(f), \beta(f)]$ terms are given as

$$Z\begin{bmatrix} 1 \\ 1 \end{bmatrix} = \sqrt{\frac{\vartheta_1}{\eta}}, \qquad Z\begin{bmatrix} 1 \\ 0 \end{bmatrix} = \sqrt{\frac{\vartheta_2}{\eta}},$$

$$Z\begin{bmatrix} 0 \\ 0 \end{bmatrix} = \sqrt{\frac{\vartheta_3}{\eta}}, \qquad Z\begin{bmatrix} 0 \\ 1 \end{bmatrix} = \sqrt{\frac{\vartheta_4}{\eta}}, \tag{6.2}$$

where ϑ_i and η are the Jacobi theta functions and the Dedekind eta function respectively. The bosonic term Z_B comes from ∂X, the bosonic superpartners of the ψ. Their contribution to the partition function in four dimensions is given by

$$Z_B = \frac{1}{\tau_2} \frac{1}{\eta^2 \bar{\eta}^2}, \tag{6.3}$$

where τ_2 is the the imaginary part of the modular parameter.

The partition function (6.1) is a function of the modular parameter $\tau = \tau_1 + i\tau_2$, which parametrises the one-loop world-sheet torus. Thus, to get a numerical value from the one-loop partition function, one has to sum over all the inequivalent tori, i.e. all values of τ that give tori that are not related by modular transformations. This region of the complex plane is referred to as the fundamental domain of the modular group and is denoted $\mathcal{F} \subset \mathbb{C}$, with

$$\mathcal{F} = \{\tau \in \mathbb{C} \,|\, |\tau|^2 > 1 \ \wedge \ |\tau_1| < 1/2\}.$$

The full partition function therefore is given by the integral of (6.1) over this domain, specifically

$$Z = \int_{\mathcal{F}} \frac{d^2\tau}{\tau_2^2} Z_B \sum_{Sp.Str.} C\begin{bmatrix} \alpha \\ \beta \end{bmatrix} \prod_f Z\begin{bmatrix} \alpha(f) \\ \beta(f) \end{bmatrix}, \tag{6.4}$$

where $d^2\tau/\tau_2^2$ is the modular invariant measure. The expression (6.4) specifically represents the one-loop vacuum energy of our theory and so we may refer to it as the cosmological constant Λ.
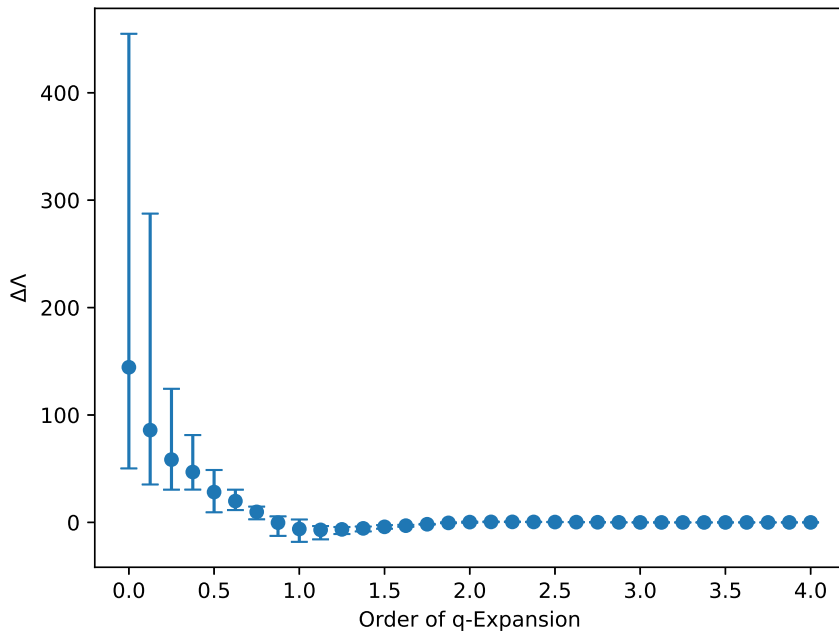
Figure 1: *The convergence of Λ order-by-order in the q-expansion, where $\Delta\Lambda$ is the difference between Λ at a specific order and Λ at 4th order. The dots represent the average over a sample of 2000 tachyon-free models and the bars give the maximum deviation from this average.*

The practical way to perform this integral is as presented in [36] using the expansion of the η and θ functions in terms of the modular parameter, or more conveniently in terms of $q \equiv e^{2\pi i \tau}$ and $\bar{q} \equiv qe^{-2\pi i \bar{\tau}}$. This leads to a series expansion of the one-loop partition function which converges quickly as demonstrated in Figure 1. The details and conventions for the q-expansions can be found in Appendix A. All terms in the partition function sum (6.4) are modular functions of the variable τ and so we can rewrite the expression in terms of a q-expansion as

$$Z = \sum_{n.m} a_{mn} \int_{\mathcal{F}} \frac{d^2\tau}{\tau_2^3} q^m \bar{q}^n = \sum_{n.m} a_{mn} \int_{\mathcal{F}} \frac{d^2\tau}{\tau_2^3} e^{-2\pi\tau_2(m+n)} e^{2\pi i\tau_1(n-m)}. \tag{6.5}$$

It is important to note, that in the expression above, the a_{mn} physically represent the difference between bosonic and fermionic degrees of freedom at each mass level, i.e. $a_{mn} = N_b - N_f$. Since the fundamental domain $\mathcal{F}$ is symmetric with respect to τ_1, only the even part of the τ_1 exponential will contribute giving

$$Z = \sum_{n.m} a_{mn} \int_{\mathcal{F}} \frac{d^2\tau}{\tau_2^3} e^{-2\pi\tau_2(m+n)} \cos(2\pi\tau_1(m-n)) =: \sum_{m,n} a_{mn} I_{mn}. \tag{6.6}$$

The integral over τ_1 can be done analytically while the τ_2 integral has to be done numerically. The analytic integral is calculated by splitting $\mathcal{F}$ into the two regions

$$\begin{cases} \mathcal{F}_1 = \{\tau \in \mathbb{C} \,|\, \tau_2 \geq 1 \ \wedge \ |\tau_1| < 1/2\} \\ \mathcal{F}_2 = \{\tau \in \mathbb{C} \,|\, |\tau|^2 > 1 \ \wedge \ \tau_2 < 1 \ \wedge \ |\tau_1| < 1/2\}, \end{cases}$$

17

such that $\mathcal{F} = \mathcal{F}_1 \cup \mathcal{F}_2$. Performing the integration over τ_2 in this way also gives insight into what terms can and cannot contribute to the partition function. The integral over $\mathcal{F}_2$ is always finite however, the integral over $\mathcal{F}_1$ diverges for specific values of m, n. We specifically find that the following cases arise:

$$I_{mn} = \begin{cases} \infty & \text{if } m + n < 0 \ \wedge \ m - n \notin \mathbb{Z}\backslash\{0\} \\ \text{Finite} & \text{Otherwise.} \end{cases} \tag{6.7}$$

The numerical values of the integrals I_{mn} can be found in Table 16 of Appendix A. We learn that as expected on-shell tachyonic states, i.e. states with $m = n < 0$, have an infinite contribution. On the other hand, it is important to note that some off-shell tachyonic states may contribute a finite value to the partition function. The above result also shows that not only on-shell tachyonic states can cause a divergence, but some off-shell tachyonic states as well. These states, however, do not arise due to the modular invariance constraints on the coefficients $C\begin{bmatrix} \alpha \\ \beta \end{bmatrix}$, which only allows states with $m - n \in \mathbb{Z}$.

The modular invariance constraint $m - n \in \mathbb{Z}$ means that the q-expansion of the partition function (6.5) neatly arranges into the form

$$a_{mn} = \begin{pmatrix} 0 & 0 & a_{-\frac{1}{2}-\frac{1}{2}} & 0 & 0 & 0 & a_{-\frac{1}{2}\frac{1}{2}} & 0 & 0 & 0 \\ 0 & 0 & 0 & a_{-\frac{1}{4}-\frac{1}{4}} & 0 & 0 & 0 & a_{-\frac{1}{4}\frac{3}{4}} & 0 & 0 \\ a_{0-1} & 0 & 0 & 0 & a_{00} & 0 & 0 & 0 & a_{01} & 0 \\ 0 & a_{\frac{1}{4}-\frac{3}{4}} & 0 & 0 & 0 & a_{\frac{1}{4}\frac{1}{4}} & 0 & 0 & 0 & \ddots \\ 0 & 0 & a_{\frac{1}{2}-\frac{1}{2}} & 0 & 0 & 0 & a_{\frac{1}{2}\frac{1}{2}} & 0 & 0 & 0 \\ 0 & 0 & 0 & a_{\frac{3}{4}-\frac{1}{4}} & 0 & 0 & 0 & a_{\frac{3}{4}\frac{3}{4}} & 0 & 0 \\ a_{1-1} & 0 & 0 & 0 & a_{10} & 0 & 0 & 0 & a_{11} & 0 \\ 0 & \ddots & 0 & 0 & 0 & \ddots & 0 & 0 & 0 & \ddots \end{pmatrix} \tag{6.8}$$

i.e. into series of states with $n - m = p \in \mathbb{Z}$. This gives a convenient way to examine the different contributions to the cosmological constant (6.6) and compare the effect of on and off-shell states. As an example we consider a model with a small value for the cosmological constant as shown Figure 2. We see that the suppressed value of Λ is due to the cancellation between the large positive contributions from the on-shell states and the negative contributions from the off-shell states. Indeed, in general we find that for our set of models, the only positive contributions to Λ come from on-shell states and so these states can give us a handle on the expected value of the cosmological constant.

As we have seen in Figure 1, for our tachyon-free models, Λ always converges and does so rapidly starting from 2nd order in q. It is often stated that the finiteness of string theory is due to supersymmetry, which in our case is not present, thus one may wonder how the partition function of non-supersymmetric theories manages to remain finite. For supersymmetric free fermionic theories the usual S-vector (2.2) ensures that the bosonic and fermionic degrees of freedom are exactly matched at each mass level. That is, for a supersymmetric theory we necessarily have that $a_{mn} = 0$ for all m and n, which in turn causes the vanishing of the cosmological constant as one expects. For our non-supersymmetric models, the lack of an S-vector means that such cancellations are not ensured and so such theories in general produce a non-zero value for Λ. It is, however, not obviously clear that they should produce finite partition functions. Such
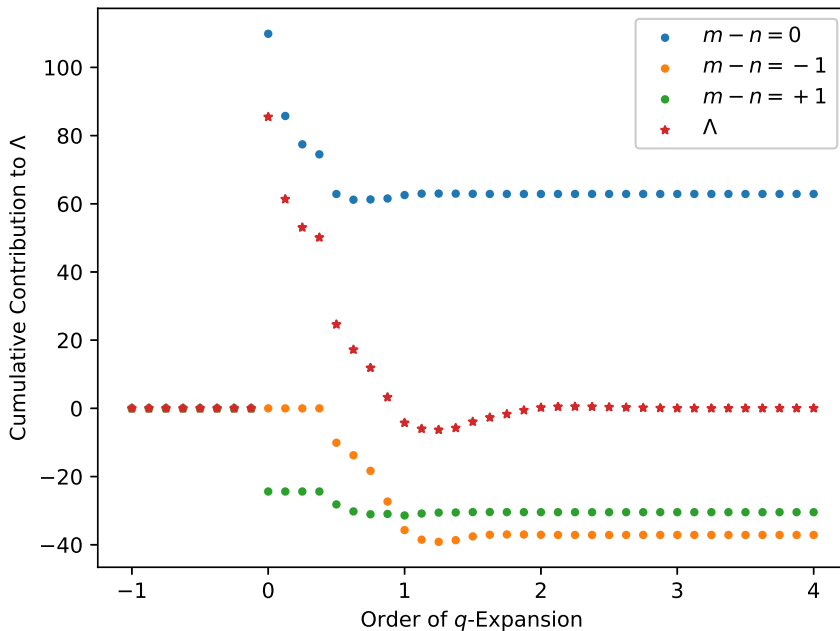
Figure 2: *A comparison of different contributions to* Λ *for a model with* $\Lambda = 0.03$ *arranged as in (6.8). We see that the large positive contributions of the on-shell states are compensated by the negative contributions of the off-shell states.*

finiteness is achieved through a mechanism called misaligned supersymmetry as presented in [40, 41, 42].

As one expects, the degeneracy of states grows rapidly going up the infinite tower of massive states. This growth, in theory, could counteract the suppression received from the decreasing contributions from the integrals in Table 16 and cause divergences. The mechanism of misaligned supersymmetry, however, causes the states in the massive tower to oscillate between an excess of bosons and an excess of fermions. This behaviour is referred to as boson-fermion oscillation. Our models indeed present this behaviour as shown in Figure 3. Instead of cancelling level-by-level as in the supersymmetric case, the cancellation is misaligned causing the oscillation meaning a large positive contribution is followed by an even larger negative contribution and so on. This mechanism ensures that the partition function of our non-supersymmetric models remains finite.

6.1 $N_b = N_f$ at the Massless Level

The discussion above shows that while for non-supersymmetric theories there is no mechanism which ensures the vanishing of a_{mn} at any allowed level, there is, however, nothing preventing it from happening. It is indeed possible to find models within our classification set-up detailed in Section 3 which have $a_{00} = 0$, *i.e.* $N_b^0 = N_f^0$.

In the analysis of the one-loop potential in [7], no models are found which exhibit $N_b^0 = N_f^0$ at the free fermionic point in the sample explored. Instead they use techniques developed in [43] to move away from the free fermionic point using an analogous orbifold rewriting of the partition function and find models with $N_b^0 = N_f^0$ at a generic point in

19
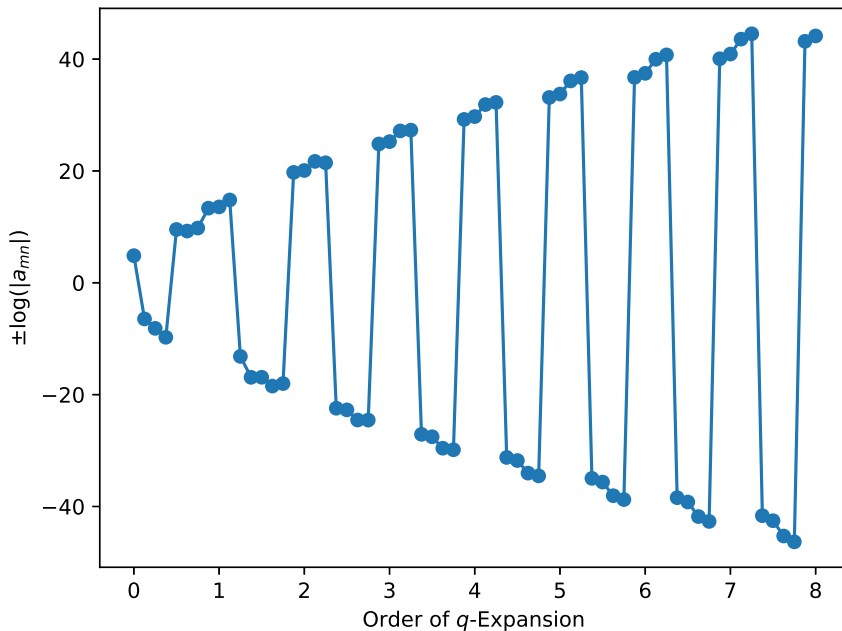
Figure 3: *The boson-fermion oscillation of misaligned supersymmetry for the on-shell states of one of our models to 8th order in the q-expansion. The overall sign of $\pm \log(| a_{mn} |)$ is chosen according to the sign of a_{mn}.*

the moduli space. In our analysis we stay at the free fermionic point and it turns out that we do find models with $N_b^0 = N_f^0$ and an example model is presented in Section 7.3.

It is convenient to summarise the various contributions to a_{00} in the form of Table 13. We use the notation for sectors laid out in Section 5. For simplicity, and since we restrict our classification to models with no enhancements, the contributions of vector bosons from sectors $z_1, z_2, z_1 + z_2$ are ignored.

Sector	$N_b - N_f$	Sector	$N_b - N_f$
$|NS\rangle$	304	$\{\bar{y}_{NS}^i/\bar{w}_{NS}^i\}|\tilde{V}\rangle$	-8
$|B^{1,2,3}\rangle$	-32	$\delta^{1,...,30}$	16
$|\tilde{x}\rangle$	-256	$\{\bar{\psi}^{a(*)}/\bar{\eta}^{b(*)}\}|\gamma^{1,...,15}\rangle$	64
$\{\bar{\psi}^{a(*)}\}|V^{1,2,3}\rangle$	32	$\{\bar{y}_{NS}^i/\bar{w}_{NS}^i\}|\gamma^{1,...,15}\rangle$	4
$\{\bar{\phi}^{\{1,2\}/\{3,4\}/\{5,6\}/\{7,8\}(*)}\}|V^{1,2,3}\rangle$	8	$\{\bar{\phi}^{\{1,2\}/\{3,4\}/\{5,6\}/\{7,8\}(*)}\}|\gamma^{1,...,15}\rangle$	8
$\{\bar{y}^i/\bar{w}^i\}|V^{1,2,3}\rangle$	4	$\{y_{NS}^i/w_{NS}^i\}\{\bar{y}_{NS}^j/\bar{w}_{NS}^j\}|z_{1/2}\rangle$	8
$|H^{1,...,6}\rangle$	16	$\{y_{NS}^i/w_{NS}^i\}\{\bar{\eta}^{b(*)}\}|z_{1/2}\rangle$	32
$|H^{7,...,18}\rangle$	-8	$\{y_{NS}^i/w_{NS}^i\}\{\phi^{\{5,6,7,8\}/\{1,2,3,4\}(*)}\}|z_{1/2}\rangle$	16
$\{\bar{\psi}^{1,...,5(*)}, \bar{\eta}^{1,2,3(*)}, \bar{\phi}_{NS}^{(*)}\}|\tilde{V}\rangle$	-192	$\{y_{NS}^i/w_{NS}^i\}|z_1 + z_2\rangle$	8

Table 13: *Contributions of massless sectors to a_{00} when present in Hilbert space of a model. As noted $a_{00} = N_b^0 - N_f^0$, so bosonic contributions are positive and fermionic are negative. The superscripts used here are $i \neq j = 1, ..., 6$, $a = 1, ..., 5$ and $b = 1, 2, 3$. The NS subscript means that the oscillator has Neveu-Schwarz boundary conditions in the sector.*

7 Results of Classification

Having discussed how to determine key features of the massless spectrum and how to calculate the partition function and cosmological constant for our $\tilde{S}$-models we can now present some statistics derived from a sample in the space of models. As mentioned in Section 3, the space of all models is $2^{66} \sim 10^{19.9}$ and so a complete classification is far beyond the computing power at our disposal. Instead, we explore a sample of 2×10^9 models of which only around 1 in 185 are tachyon-free that we take forward for further analysis. We will start with some results of key aspects of the massless spectrum.

7.1 Results from Massless Spectrum

From our sample of 2×10^9 models we choose 10^7 tachyon-free models and display the results for their $SO(10)$ observable representations. In Figure 4 the net chirality, $N_{16} - N_{\overline{16}}$, distribution is displayed and in Figure 5 the distribution of their number of vectorial **10** representations is displayed. The familiar normal distribution also found in all other
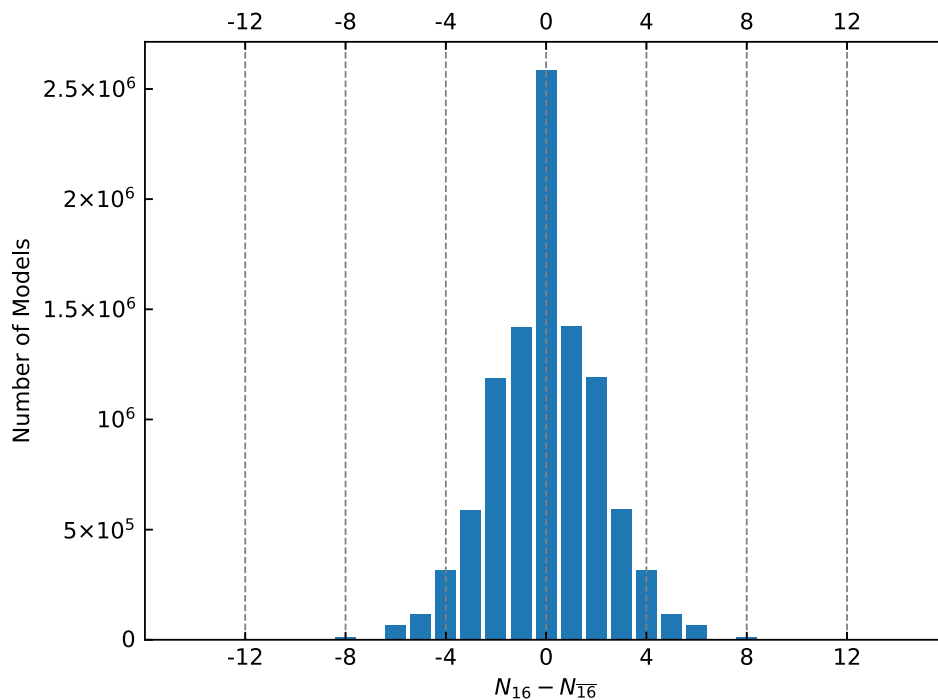
Figure 4: *Number of models versus net chiral generations from a random sample of* 10^7 *tachyon free* $SO(10)$ *models.*

classifications for the supersymmetric cases is uncovered. This is hardly surprisingly since the structure of the fermionic **16**/**$\overline{16}$** is unchanged for our models. From Figure 5 we see that the large majority of models contain at least 1 vectorial **10** which may be used to generate a bidoublet Higgs representation when the $SO(10)$ is broken.

In order to see more clearly the statistics from our 2×10^9 sample we display the frequency of $SO(10)$ models as several phenomenological constraints are considered in Table 14.
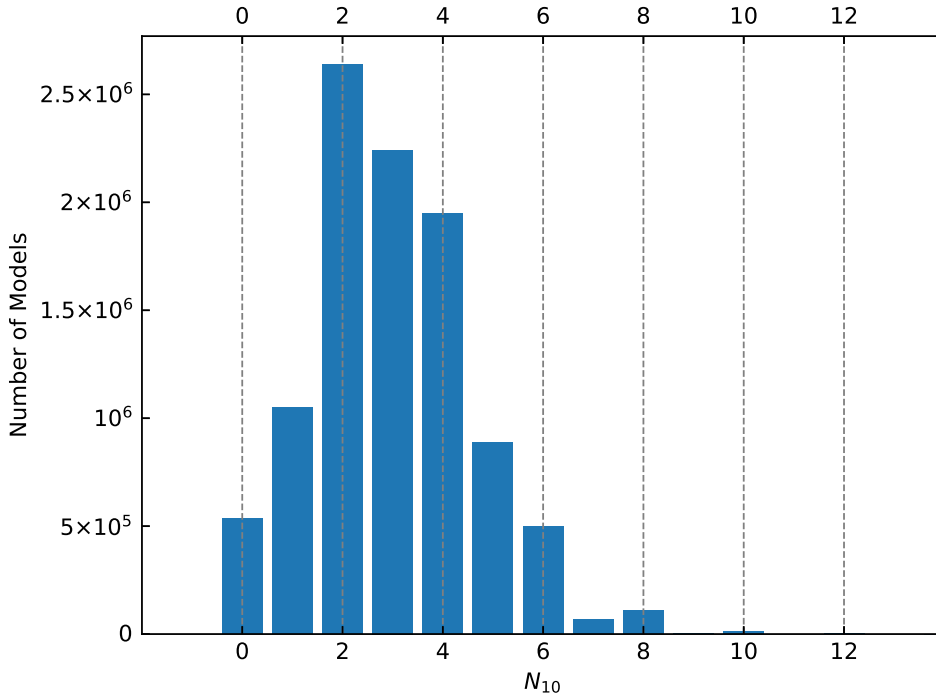
Figure 5: *Number of models versus number of vectorial* **10** *sectors from a random sample of* 10^7 *tachyon free* $SO(10)$ *models.*

	Constraints	Total models in sample	Probability
	No Constraints	2×10^9	1
(1)	+ Tachyon-Free	10741667	5.37×10^{-3}
(2)	+ No Observable Enhancements	10741667	5.37×10^{-3}
(3)	+ No Hidden Enhancements	9921843	4.96×10^{-3}
(4)	+ $N_{16} - N_{\overline{16}} \geq 6$	69209	3.46×10^{-5}
(5)	+ $N_{10} \geq 1$	69013	3.45×10^{-5}
(6)	+ $a_{00} = N_b^0 - N_f^0 = 0$	3304	1.65×10^{-6}

Table 14: *Phenomenological statistics from sample of* 2×10^9 $SO(10)$ $\tilde{S}$-*models.*

These results confirm the observation made in previous sections that there are no tachyon-free models in our construction which have observable enhancements. In phenomenological terms, we do not need to worry about enhancements of the hidden sector gauge group, but they are included in the table for completeness. The next constraints we add are much like the so-called 'fertility constraints' implemented in [22, 25]. The constraint on the net chirality $N_{16} - N_{\overline{16}} \geq 6$ is a necessary, but not sufficient, condition for the existence of 3 or more chiral generations at the level of the standard model. The condition $N_{10} \geq 1$ ensures at least one state exists that can produce a Standard Model Higgs doublet and can be used to break the electroweak symmetry. Finally, we implement a condition on the q-expansion coefficient $a_{00} = 0$ which corresponds to finding models with $N_b = N_f$ at the massless level as discussed in Section 6.

The 3304 models satisfying all these constraints are notable, particularly in regard to this final condition of $N_b^0 = N_f^0$. Inspecting the patterns in the spectra of these 3304
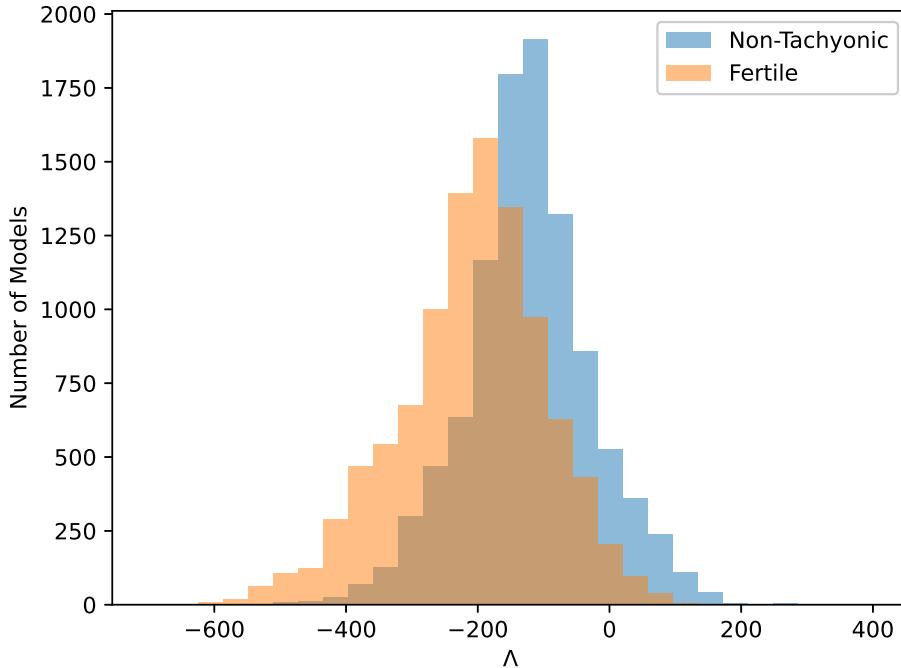
Figure 6: *The distribution of the cosmological constant for a sample of 10^4 non-tachyonic and 10^4 fertile models models.*

models revealed that $\sim 58\%$ contain the vector $\tilde{x}$ in their spectrum. In these cases the large negative contribution of -256 that $\tilde{x}$ contributes to a_{00} is helpful in ensuring $N_b^0 = N_0^f$. Of those models not containing $\tilde{x} \sim 70\%$ obtained the large negative contribution of -192 from one of the additional vectorials $\tilde{V} = \tilde{S}, \tilde{S} + z_1, \tilde{S} + z_2, \tilde{S} + z_1 + z_2$ with mixed charges under the observable and hidden groups, i.e. the sectors $\{\bar{\psi}^{1,\ldots,5}, \bar{\eta}^{1,2,3}, \bar{\phi}_{NS}\} |\tilde{V}\rangle$. Again this large negative contribution helps in matching the number of massless fermions to massless bosons.

7.2 Results for Cosmological Constant and $N_b^0 - N_f^0$

As the value of the constant term $a_{00} = N_b^0 - N_f^0$ and the cosmological constant Λ vary from model-to-model, it is interesting to see what range of values these non-supersymmetric models can produce.

The distribution of the cosmological constant Λ is shown in in Figure 6, for a sample of 10^4 non-tachyonic and 10^4 fertile models. By non-tachyonic we mean that only condition (1) of Table 14 is satisfied, while fertile models satisfy all conditions (1)-(5). It is important to note that values presented in Figure 6 are at the special free fermionic point in moduli space. This means that moving away from this point will change these values and if there are unfixed moduli, there is nothing preventing this from happening. This is indeed the case for our class of models.

Another interesting quantity in the partition functions is boson-fermion degeneracy at the massless level. As discussed in Section 6, the on-shell states provide the majority of positive contributions to the partition function, the largest of which is the massless term.
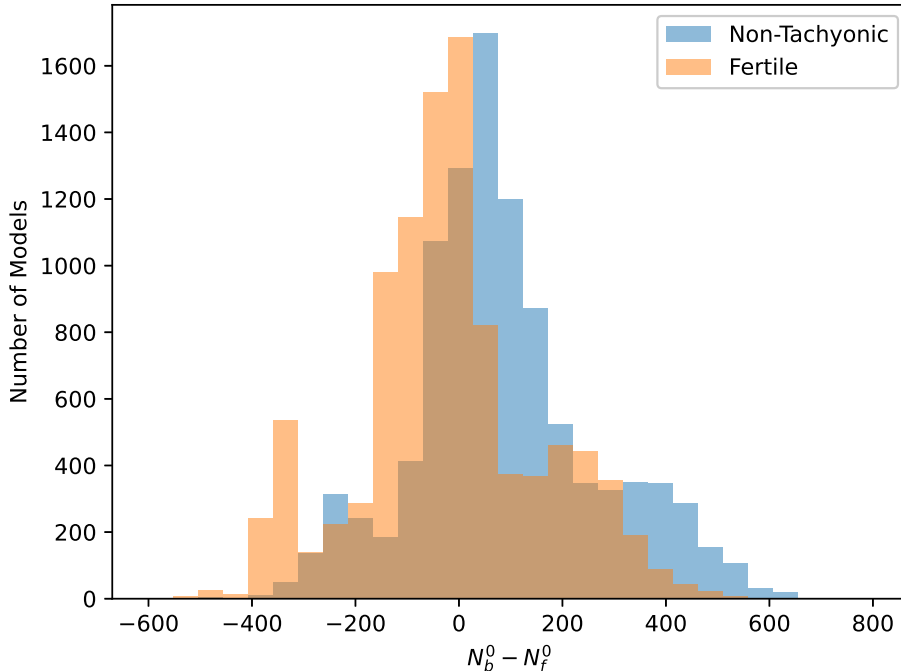
Figure 7: *The distribution of the constant term $a_{00} = N_b^0 - N_f^0$ for a sample of 10^4 non-tachyonic and 10^4 fertile models.*

Thus the value of a_{00} gives a good handle on the value of the cosmological constant. It is also, of course, interesting for the discussion of phenomenological features and stability as explained in Section 6.1. The distribution of values of $a_{00} = N_b^0 - N_f^0$ for a sample of 10^4 non-tachyonic and 10^4 fertile models is shown in Figure 7.

From Figures 6 and 7 we see that the fertility conditions have a measurable effect on the distribution of Λ and a_{00}, that is, they slightly shift the values of both to the negative. This is an interesting effect and is likely due to condition (4) in Table 14. Even though the fertility condition (4) is directed at ensuring the difference $N_{16} - N_{\overline{16}}$ is greater than 6, in doing this it also results in fertile models having a larger average total $N_{16} + N_{\overline{16}}$ compared to non-fertile models. As specified in Table 13, these sectors contribute a value of -32 to a_{00} and thus appear to cause the shift toward smaller values for a_{00} and as a consequence also for Λ.

7.3   A Model with $N_b^0 = N_f^0$

From the 3304 fertile models with $N_b^0 = N_f^0$ we present an analysis of the key features of the massless spectrum for one example model, as well as presenting its partition function

and cosmological constant. The model we choose has the GGSO matrix

$$
C\begin{bmatrix} v_i \\ v_j \end{bmatrix} =
\begin{array}{c}
\\ \mathbf{1} \\ \tilde{S} \\ e_1 \\ e_2 \\ e_3 \\ e_4 \\ e_5 \\ e_6 \\ b_1 \\ b_2 \\ b_3 \\ z_1
\end{array}
\begin{array}{c}
\begin{array}{cccccccccccc}
\mathbf{1} & \tilde{S} & e_1 & e_2 & e_3 & e_4 & e_5 & e_6 & b_1 & b_2 & b_3 & z_1
\end{array} \\
\left(
\begin{array}{cccccccccccc}
-1 & -1 & 1 & -1 & -1 & -1 & 1 & 1 & 1 & 1 & -1 & -1 \\
-1 & 1 & -1 & -1 & -1 & 1 & 1 & 1 & 1 & -1 & -1 & 1 \\
1 & -1 & -1 & -1 & -1 & -1 & -1 & -1 & -1 & -1 & -1 & 1 \\
-1 & -1 & -1 & 1 & -1 & 1 & 1 & -1 & 1 & -1 & 1 & -1 \\
-1 & -1 & -1 & -1 & 1 & -1 & -1 & 1 & 1 & 1 & -1 & -1 \\
-1 & 1 & -1 & 1 & -1 & 1 & 1 & 1 & 1 & -1 & 1 & 1 \\
1 & 1 & -1 & 1 & -1 & 1 & -1 & 1 & -1 & 1 & 1 & -1 \\
1 & 1 & -1 & -1 & 1 & 1 & 1 & -1 & -1 & 1 & 1 & 1 \\
1 & -1 & -1 & 1 & 1 & 1 & -1 & -1 & 1 & -1 & 1 & 1 \\
1 & 1 & -1 & -1 & 1 & -1 & 1 & 1 & -1 & 1 & -1 & 1 \\
-1 & 1 & -1 & 1 & -1 & 1 & 1 & 1 & 1 & -1 & -1 & -1 \\
-1 & -1 & 1 & -1 & -1 & 1 & -1 & 1 & 1 & 1 & -1 & -1
\end{array}
\right)
\end{array}
\tag{7.1}
$$

This model has $N_{16} = 7$, $N_{\overline{16}} = 1$ and $N_{10} = 8$ and thus satisfies the constraints imposed in Table 14. Furthermore, in this model the $\tilde{x}$–sector produces massless states, which in the supersymmetric models would correspond to the presence of the $S + x$ sector when x enhances the $SO(10)$ symmetry to E_6. In that case, the $S + x$ include the superpartners of the gauge vector bosons of the sector x, i.e. the gauginos. So in this case, we have the gauginos but not the vector bosons.

Our model also contains 6 bosonic hidden states from the sectors $H^{1,\dots,6}$ and 48 fermionic hidden states from the $H^{7,\dots,18}$. There are additional vectorials from the sectors $e_3 + e_4 + e_5 + e_6$, $e_1 + e_2 + e_3 + e_6$ and $e_1 + e_2 + e_3 + e_4$ with observable oscillators $\{\bar{\psi}^a, \bar{\eta}^b\}$, $a = 1, \dots, 5$, $b = 1, 2, 3$ which cannot couple with observable states from $B^{1,2,3}$ since it cannot conserve the charges of the $U(1)_{1,2,3}$ in particular. However, these three sectors may provide couplings at higher order.

The partition function is calculated in terms of its q-expansion and so it can be specified by a matrix of coefficients a_{mn} as in (6.8). For our example model these values are presented in Table 15. We see that indeed this model has $a_{00} = N_b^0 - N_f^0 = 0$ as advertised

	-1	-7/8	-3/4	-5/8	-1/2	-3/8	-1/4	-1/8	0	1/8	1/4	3/8	1/2	5/8	3/4	7/8
-1/2	0	0	0	0	0	0	0	0	0	0	0	0	320	0	0	0
-3/8	0	0	0	0	0	0	0	0	0	0	0	0	0	896	0	0
-1/4	0	0	0	0	0	0	0	0	0	0	0	0	0	0	5696	0
-1/8	0	0	0	0	0	0	0	0	0	0	0	0	0	0	0	29312
0	2	0	0	0	0	0	0	0	0	0	0	0	0	0	0	0
1/8	0	0	0	0	0	0	0	0	0	-288	0	0	0	0	0	0
1/4	0	0	0	0	0	0	0	0	0	0	-4512	0	0	0	0	0
3/8	0	0	0	16	0	0	0	0	0	0	0	-9808	0	0	0	0
1/2	0	0	0	0	224	0	0	0	0	0	0	0	1344	0	0	0
5/8	0	0	0	0	0	416	0	0	0	0	0	0	0	36640	0	0
3/4	0	0	0	0	0	0	576	0	0	0	0	0	0	0	78080	0
7/8	0	0	0	0	0	0	0	-320	0	0	0	0	0	0	0	212928
1	32	0	0	0	0	0	0	0	-1440	0	0	0	0	0	0	0

Table 15: *The q-expansion of the partition function for our example model. Each entry in the table represents the coefficient a_{mn} in the partition function sum (6.5), with the first column and row being the mass levels for the left and right moving sectors respectively.*

and the series of states arrange according to (6.8). The absence of on-shell tachyons is explicit and the contribution from off-shell tachyonic states is non-zero as expected. We also find that the consistency condition $a_{0-1} = 2$ for the proto-graviton (4.2) as described in [6, 36] is also satisfied.

The cosmological constant can also be calculated according to (6.6) with the modular integral quickly converging after 2nd order in q. In this case it takes the value

$$\Lambda = \sum_{m,n} a_{mn} I_{mn} = -149.77 \tag{7.2}$$

at the free fermionic point. As we see it is negative which is the case for most models with $N_b^0 = N_f^0$. This is due to the fact that the largest positive contributions to the partition function come from the light on-shell states and in particular from the massless states. If $N_b^0 - N_f^0 = 0$, this is zero and the negative contributions from the light off-shell tachyons produce a negative value for Λ. This is indeed the case for all 3304 such models in our scan.

8 Discussion and Conclusion

In this paper we developed systematic computerised tools to classify large spaces of free fermion heterotic string vacua that correspond to compactifications of ten dimensional tachyonic vacua. From the point of view of the four dimensional constructions this is achieved by the general $\tilde{S}$–map. Our previous $\overline{\text{NAHE}}$–based model [11] was similarly constructed from the model published in [45], which raises the question what are the consequences of applying the map to generic models, *i.e.* what are the relations between the spectra of the two mapped models, and what are the general patterns. This relation is similar to the general relation exhibited by the spinor–vector duality map, and the two may in fact be manifestation of a much larger symmetry structure [35].

Adopting the classification methodology developed for supersymmetric free fermionic models entails the proliferation of tachyon producing sectors in the $\tilde{S}$–mapped models. The systematic classification therefore requires detailed analysis of these sectors that was discussed in Section 4. In the analysis of the massless sectors separate attention to bosonic and fermionic sectors is required and was discussed in Section 5. In Section 6 we discussed the general analysis of the partition function and its q–expansion in left and right moving energy modes. The analysis of the partition function is particularly instrumental in the case of non–supersymmetric string vacua as it gives a direct handle on the physical states at different mass levels. Of particular interest in the q–expansion is the $a_{00} = N_b^0 - N_f^0$ term, which counts the difference between massless bosons and fermions in the spectrum of the string vacuum. In supersymmetric models the number of fermionic and bosonic degrees of freedom are matched at all mass levels, and hence the partition function and the vacuum energy are identically zero. In non–supersymmetric models there is a generic mismatch at different mass levels, which is partially compensated by the so–called misaligned supersymmetry [41]. It has been argued that in tachyon–free non–supersymmetric models with $a_{00} = 0$ the vacuum energy may be suppressed by the volume of the compactified dimensions [46].

In Section 7 we presented the results of the classification of the order of 2×10^9 random GGSO phases that generate the space of vacua spanned by the basis vectors in eq. (3.1) and the 66 independent one–loop GGSO phases. The analysis reveals that tachyon–free

27

models occur with $\sim 5 \times 10^{-3}$ probability. Furthermore, we analysed this data by further imposing some fertility conditions $N_{16} - N_{\overline{16}} \geq 6$ and $N_{10} \geq 1$ and found fertile models with $a_{00} = 0$ with frequency $\sim 2 \times 10^{-6}$ in our sample. In Figures 7 and 6 a notable shift in values of the cosmological constant and the a_{00} term were detected for fertile models compared with a random sample of non-tachyonic vacua.

These results reveal that extracting interesting phenomenological models necessitates the development of more sophisticated computerised methods than the random generation method. This is particularly true in light of the fact that generating viable symmetry breaking pattern may necessitate breaking the $SO(10)$ symmetry to the Standard Model subgroup. The $\tilde{S}$–map entails that scalar degrees of freedom in the spinorial sixteen representation of $SO(10)$ are shifted to the massive spectrum. The consequence is that the spectrum does not contain the neutral component in the 16 of $SO(10)$ required to break the remnant unbroken gauge symmetry down to the Standard Model gauge group. The only available states are exotic states that carry fractional $U(1)_{Z'}$ charge and appear in the heterotic string Standard–like Models [47]. This assertion requires of course further investigation that will be scrutinised in future work. The lesson may be that quasi–realistic models in this class may only be possible for a very restricted and narrow set of models, rather than the more generic set, which is the prevalent experience with supersymmetric constructions. In forthcoming work these questions are investigated in tachyon–free Pati–Salam models, including the inclusion of fertility conditions. The increased space of vacua, in particular in the case of Standard–like models, requires adaptation of novel computational techniques [33].

Following from or previous paper [11] the analysis and results presented in this work open up new vistas in string phenomenology. It reveals the potential relevance of string vacua that have been previously considered to be irrelevant. The number of questions to explore is large and may potentially provide insight into some of the prevailing problems in string phenomenology. Interpolation between the supersymmetric vacua and our tachyon–free constructions, as well as with the two dimensional MSDS constructions [48], may shed some light on the problem of supersymmetry breaking and vacuum energy in string theory. This can be carried out in a subset of the basis vectors $e.g.$ $\{1, \tilde{S}, b_1\}$ or $\{1, \tilde{S}, \tilde{x}\}$. Another question of interest is the question of stability of the tachyon–free models. This question is necessarily tied with the non–vanishing one–loop vacuum energy in these models. In this respect it will be interesting to analyse the one–loop diagram that arises in these models due to the existence of an anomalous $U(1)$ symmetry [49] and to examine whether two diagrams can be cancelled against each other. Finally, further understanding of the symmetries that underlie the partition function at all mass levels, as exhibited at the massless level by the $\tilde{S}$ and $\tilde{x}$ maps, are important to extract.

Acknowledgments

A   Theta Functions and Integrals

As we have seen, the partition functions are given in terms of Jacobi theta and Dedekind eta functions. These are the functions that we have to expand in terms of the parameters $q \equiv e^{2\pi i \tau}$ and $\bar{q} \equiv q e^{-2\pi i \bar{\tau}}$ in order to perform the integrals over the modular domain. Further details can be found in [50], and for completeness we list below the q-expansions used to calculate the partition function.

The q-expansions of the θ and η functions are easily derived form their definitions

$$\vartheta_2 = \sum_{n \in \mathbb{Z}} q^{(n+1/2)^2/2} = 2q^{1/8} + 2q^{9/8} + 2q^{25/8} + \cdots \tag{A.1}$$

$$\vartheta_3 = \sum_{n \in \mathbb{Z}} q^{n^2/2} = q^0 + 2q^{1/2} + 2q^2 + \cdots \tag{A.2}$$

$$\vartheta_4 = \sum_{n \in \mathbb{Z}} (-1)^n q^{n^2/2} = q^0 - 2q^{1/2} + 2q^2 + \cdots \tag{A.3}$$

$$\eta = q^{1/24} \prod_{n=1}^{\infty} (1 - q^n) = q^{1/24} - q^{25/24} - q^{49/24} + \cdots . \tag{A.4}$$

Since the partition function only involves negative powers of η, the above expression is not useful in practical terms. One can, however, find a general expansion for η^{-1} using the multinomial theorem which gives

$$\eta^{-1} = q^{-1/24} \prod_{n=1}^{\infty} \sum_{k=0}^{\infty} \binom{-1}{k} (-1)^k q^{nk} = q^{-1/24} + q^{23/24} + 2q^{47/24} + \cdots . \tag{A.5}$$

Substituting the above q-expansions into the partition function we arrive at the form stated in (6.5) and thus all that remains is to calculate the integrals of the form

$$I_{mn} = \int_{\mathcal{F}} \frac{d^2\tau}{\tau_2^3} \, q^m \bar{q}^n = \int_{\mathcal{F}} \frac{d^2\tau}{\tau_2^3} \, e^{-2\pi \tau_2(m+n)} e^{2\pi i \tau_1(n-m)}. \tag{A.6}$$

As described above in Section 6, this is done using both analytic an numerical techniques. The values of these integrals can be found in Table 16, where they are listed for the range $m, n \leq 1$.

$q\backslash\bar{q}$	-1	- 3/4	- 1/2	- 1/4	0	1/4	1/2	3/4	1
-1	∞	∞	∞	∞	-1.22×10^{1}	∞	∞	∞	9.90×10^{-3}
- 3/4	∞	∞	∞	∞	∞	-6.17×10^{-1}	∞	-1.34×10^{-1}	-8.55×10^{-3}
- 1/2	∞	∞	∞	∞	∞	∞	-3.15×10^{-2}	-1.78×10^{-2}	-2.98×10^{-3}
- 1/4	∞	∞	∞	∞	∞	3.35×10^{-1}	1.30×10^{-2}	-1.63×10^{-3}	-6.47×10^{-4}
0	-1.22×10^{1}	∞	∞	∞	5.49×10^{-1}	5.56×10^{-2}	5.61×10^{-3}	2.25×10^{-4}	-8.46×10^{-5}
1/4	∞	-6.17×10^{-1}	∞	3.35×10^{-1}	5.56×10^{-2}	1.00×10^{-2}	1.54×10^{-3}	1.70×10^{-4}	3.21×10^{-6}
1/2	∞	∞	-3.15×10^{-2}	1.30×10^{-2}	5.61×10^{-3}	1.54×10^{-3}	3.30×10^{-4}	5.52×10^{-5}	6.05×10^{-6}
3/4	∞	-1.34×10^{-1}	-1.78×10^{-2}	-1.63×10^{-3}	2.25×10^{-4}	1.70×10^{-4}	5.52×10^{-5}	1.29×10^{-5}	2.22×10^{-6}
1	9.90×10^{-3}	-8.55×10^{-3}	-2.98×10^{-3}	-6.47×10^{-4}	-8.46×10^{-5}	3.21×10^{-6}	6.05×10^{-6}	2.22×10^{-6}	5.47×10^{-7}

Table 16: *The values of the integral I_{mn} for $m, n \leq 1$. The first column and row denotes the value of m and n respectively.*

References

[1] P. Candelas, G.T. Horowitz, A. Strominger and E. Witten, *Nucl. Phys.* **B258** (1985) 46;
D.J. Gross, J.A. Harvey, E.J. Martinec and R. Rohm, *Nucl. Phys.* **B267** (1986) 75.

[2] L.J. Dixon, J.A. Harvey, *Nucl. Phys.* **B274** (1986) 93;
L. Alvarez–Gaume, P.H. Ginsparg, G.W. Moore and C. Vafa, *Phys. Lett.* **B171** (1986) 155.

[3] H. Itoyama and T.R. Taylor, *Phys. Lett.* **B186** (1987) 129.

[4] K.R. Dienes, *Phys. Rev. Lett.* **65** (1990) 1979; *Phys. Rev.* **D42** (1990) 2004;
S. Abel and K.R. Dienes, *Phys. Rev.* **D91** (2015) 126014;
K.R. Dienes, *Phys. Rev.* **D73** (2006) 1006010;
M. Blaszczyk, S. Groot Nibbelink, O. Loukas and F. Ruehle,*JHEP* **1510** (2015) 166;
S. Groot Nibbelink and E. Parr, *Phys. Rev.* **D94** (2016) 041704;
S. Groot Nibbelink *et al*, arXiv:1710.09237;
T. Coudarchet and H. Partouche, *Nucl. Phys.* **B933** (2018) 134;
A. Abel, E. Dudas, D. Lewis and H. Partouche, arXiv:1812.09714;
H. Itoyama and S. Nakajima, *Prog. of Th. and Exp. Phys.* **12** (2019) 123B01;
H. Itoyama and S. Nakajima, arXiv:2003.11217;
M. McGuigan, arXiv:1907.01944.

[5] J.M. Ashfaque, P. Athanasopoulos, A.E. Faraggi and H.Sonmez, *Eur. Phys. Jour.* **C76** (2016) 208.

[6] S. Abel, K.R. Dienes and E. Mavroudi, *Phys. Rev.* **D97** (2018) 126017;

[7] I. Florakis and J. Rizos, *Nucl. Phys.* **B913** (2016) 495;

[8] H. Kawai, D.C. Lewellen and S.H.H. Tye, *Phys. Rev.* **D34** (1986) 3794.

[9] P.H. Ginsparg and C. Vafa, *Nucl. Phys.* **B289** (1986) 414.

[10] A.E. Faraggi, *Eur. Phys. Jour.* **C79** (2019) 703.

[11] A.E. Faraggi, V.G. Matyas and B. Percival *Eur. Phys. Jour.* **C80** (2020) 337.

[12] N.V. Krasnikov, *Phys. Lett.* **B193** (1987) 37;
L.J. Dixon, Supersymmetry Breaking in String Theory, in The Rice Meeting: Proceedings, B. Bonner and H. Miettinen, eds., World Scientific (Singapore) 1990.

[13] I. Antoniadis, C. Bachas, and C. Kounnas, *Nucl. Phys.* **B289** (1987) 87;
H. Kawai, D.C. Lewellen, and S.H.-H. Tye, *Nucl. Phys.* **B288** (1987) 1;
I. Antoniadis and C. Bachas, *Nucl. Phys.* **B298** (1988) 586.

[14] I. Antoniadis, J. Ellis, J. Hagelin and D.V. Nanopoulos, *Phys. Lett.* **B231** (1989) 65.

[15] A.E. Faraggi, D.V. Nanopoulos and K. Yuan, *Nucl. Phys.* **B335** (1990) 347;
A.E. Faraggi, *Phys. Rev.* **D46** (1992) 3204;
G.B. Cleaver, A.E. Faraggi and D.V. Nanopoulos, *Phys. Lett.* **B455** (1999) 135.

[16] I. Antoniadis. G.K. Leontaris and J. Rizos, *Phys. Lett.* **B245** (1990) 161;
G.K. Leontaris and J. Rizos, *Nucl. Phys.* **B554** (1999) 3.

[17] A.E. Faraggi, *Phys. Lett.* **B278** (1992) 131; *Nucl. Phys.* **B387** (1992) 239;
A.E. Faraggi, E. Manno and C.M. Timirgaziu, *Eur. Phys. Jour.* **C50** (2007) 701.

[18] G.B. Cleaver, A.E. Faraggi and C. Savage, *Phys. Rev.* **D63** (2001) 066001;
G.B. Cleaver, D.J Clements and A.E. Faraggi, *Phys. Rev.* **D65** (2002) 106003.

[19] A. Gregori, C. Kounnas and J. Rizos, *Nucl. Phys.* **B549** (1999) 16.

[20] B. Assel *et al*, *Phys. Lett.* **B683** (2010) 306; *Nucl. Phys.* **B844** (2011) 365;
C. Christodoulides, A.E. Faraggi and J. Rizos, *Phys. Lett.* **B702** (2011) 81.

[21] L. Bernard *et al*, *Nucl. Phys.* **B868** (2013) 1.

[22] A.E. Faraggi, J. Rizos and H. Sonmez, *Nucl. Phys.* **B886** (2014) 202;
H. Sonmez, *Phys. Rev.* **D93** (2016) 125002.

[23] A.E. Faraggi, J. Rizos and H. Sonmez, *Nucl. Phys.* **B927** (2018) 1.

[24] A.E. Faraggi, G. Harries and J. Rizos, *Nucl. Phys.* **B936** (2018) 472.

[25] A.E. Faraggi, G. Harries, B. Percival and J. Rizos *Nucl. Phys.* **B953** (2020) 114969.

[26] A.E. Faraggi, *Phys. Lett.* **B326** (1994) 62;
E. Kiritsis and C. Kounnas, *Nucl. Phys.* **B503** (1997) 117;
A.E. Faraggi, S. Forste and C. Timirgaziu, *JHEP* **0608** (2006) 057;
P. Athanasopoulos, A.E. Faraggi, S. Groot Nibbelink and V.M. Mehta, *JHEP* **1604** (2016) 038.

[27] A. Taormina and K. Wendland, *JHEP* **2020** (2020) 184.

[28] A.E. Faraggi and D.V. Nanopoulos, *Phys. Rev.* **D48** (1993) 3288;
A.E. Faraggi, *Int. J. Mod. Phys.* **A14** (1999) 1663.

[29] A.E. Faraggi, C. Kounnas, S.E.M Nooij and J. Rizos, hep-th/0311058; *Nucl. Phys.* **B695** (2004) 41.

[30] A.E. Faraggi, C. Kounnas and J. Rizos, *Phys. Lett.* **B648** (2007) 84; *Nucl. Phys.* **B774** (2007) 208; *Nucl. Phys.* **B799** (2008) 19.

[31] T. Catelin-Julian, A.E. Faraggi, C. Kounnas and J. Rizos, *Nucl. Phys.* **B812** (2009) 103;
C. Angelantonj, A.E. Faraggi and M. Tsulaia, *JHEP* **1007** (2010) 4.

[32] A.E. Faraggi, I. Florakis, T. Mohaupt and M. Tsulaia, *Nucl. Phys.* **B848** (2011) 332.

[33] A.E. Faraggi, G. Harries, B. Percival and J. Rizos, arXiv:1901.04448.

[34] A.E. Faraggi and M. Tsulaia, *Phys. Lett.* **B683** (2010) 314;
B. Aaronson, S. Abel and E. Mavroudi, *Phys. Rev.* **D95** (2017) 106001.

[35] P. Athanasopoulos and A.E. Faraggi, *Adv. Math. Phys.* **2017** (2017) 3572469.

[36] K.R. Dienes, *Phys. Rev. Lett.* **65** (1990) 1979.

[37] G. Cleaver and A.E. Faraggi, *Int. J. Mod. Phys.* **A14** (1999) 2335.

[38] A.E. Faraggi, *Nucl. Phys.* **B407** (1993) 57; *Eur. Phys. Jour.* **C49** (2007) 803.

[39] A.E. Faraggi, C. Kounnas and H. Partouche, *Nucl. Phys.* **B899** (2015) 328.

[40] K.R. Dienes, *Nucl. Phys.* **B429** (1994) 533.

[41] K.R. Dienes, M. Moshe, and R.C. Myers, *Phys. Rev. Lett.* **74** (1995) 4767.

[42] C. Angelantonj, M. Cardella, S. Elitzur and E. Rabinovici, *JHEP* **2** (2011) 24.

[43] I. Florakis, *Nucl. Phys.* **B916** (2017) 484;

[44] A.E. Faraggi and E. Halyo, *Phys. Lett.* **B311** (1993) 307;
C. Coriano and A.E. Faraggi, *Phys. Lett.* **B581** (2004) 99.

[45] G. Cleaver, A.E. Faraggi, E. Manno and C. Timirgaziu, *Phys. Rev.* **D78** (2008) 046009.

[46] *see e.g.*: C. Kounnas and H. Partouche, *Nucl. Phys.* **B913** (2016) 593.

[47] A.E. Faraggi, *Phys. Rev.* **D46** (1992) 3204;
S. Chang, C. Coriano and A.E. Faraggi, *Nucl. Phys.* **B477** (1996) 65;
L. Delle Rose, A.E. Faraggi, C. Marzo and J. Rizos, *Phys. Rev.* **D96** (2017) 055025.

[48] C. Kounnas, *Fortsch. Phys.* **56** (2008) 1143;
I. Florakis and C. Kounnas, *Nucl. Phys.* **B820** (2009) 237;
I. Florakis, C. Kounnas and N. Toumbas, *Nucl. Phys.* **B834** (2010) 273.

[49] J.J. Atick, L.J. Dixon and A. Sen, *Nucl. Phys.* **B292** (1987) 109.

[50] S. Kharchev and A. Zabrodin, *Jour. of Geom. and Phys.* **94** (2015) 19.